W-WO_2 and W-WO_3 Oxygen Fugacity Relationship at High Temperature and Pressure

Geol394 Thesis
TJ Deane

Advisor: Dr. Andrew Campbell

1. Abstract

There are elements within the Earth that partition between both the iron rich core and the silicate portion of the Earth. Understanding the behavior of these elements under specific redox conditions can help to lead to a better understanding of how these elements behaved and partitioned themselves during core-mantle separation in the early stages of Earth's evolution. Tungsten is one of these partly siderophile, partly lithophile elements that are found in both the core and silicate Earth. In addition, some scientists use the tungsten-tungsten oxide buffer to control the oxygen fugacity in experiments at high pressures, and understanding the effect that high pressure has on this buffer is important to better control the experiments. I have studied tungsten and tungsten oxide in an attempt to evaluate their physical response to high temperatures and pressures. I have experimented with tungsten and tungsten oxide in a diamond anvil cell with a specially designed heater while using x-ray diffraction techniques to analyze the phases. For a given temperature and pressure, the crystallographic structures of the metal and the oxide have a specific volume, and that volume changes as the temperature and pressure conditions change. By understanding how the x-ray diffraction patterns change we can measure how the size of the unit cell changes with temperature and pressure. The equation of state of a material expresses the relationship among pressure, temperature, and the volume of a phase. This equation of state is applied to an equation for Gibbs free energy to calculate Gibbs free energy at high pressure. The difference between the Gibbs free energies for the tungsten metal and tungsten oxide is then related to an oxygen fugacity term which is plotted against temperature to create what is called a buffer curve. I plotted buffer curves for both WO_2 and WO_3 at varying pressures to observe how they change as I simulate conditions deeper within the Earth. At 1 bar of pressure, the WO_2 curve plots below the WO_3 curve, meaning WO_2 should be more prevalent at Earth surface, but research suggests that may not be the case. As the pressure is increased, the distance between the WO_2 curve and the WO_3 curve increases. This suggests that as the pressure is increased, the WO_2 phase becomes more and more stable relative to WO_3.

2. Introduction

Elements within the Earth can be split into two main categories: lithophile elements and siderophile elements. Lithophile elements are concentrated within the silicate portion of the Earth, and siderophile elements are concentrated within the iron-rich core of the Earth. There are some elements, however, that are partly lithophile and partly siderophile; that is, they are found in some quantity in both. Understanding why and how these elements partition between the metallic core and the silicate portions of the Earth is an ongoing investigation (Righter et al., 2003). Part of the method to solving this investigation involves trying to understand the physical and chemical properties of each of these moderately siderophile elements under a wide range of external environmental conditions such as large changes in temperature and pressure. Iron is an example of an element that is both lithophile and siderophile. Other moderately siderophile elements are chromium, manganese, nickel, and tungsten, along with other transition metals (Righter et al., 2003).

The chemical and physical properties of the tungsten-oxygen system are not well determined at high temperatures and pressures. There is an established equation of state for tungsten metal which is believed to be accurate, but there is no good model for tungsten dioxide

or tungsten trioxide. An equation of state relates the molar volume of a material to temperature and pressure. Having an accurate, well-established equation of state is important in determining other chemical properties of a material. Using the equation of state, Gibbs free energy is calculated for phases in a system. The oxygen fugacity (fO_2) is a measure of the chemical potential of O_2, or how readily the metal will react with oxygen to form its oxide. An oxygen fugacity buffer curve plots $\ln fO_2$ against temperature for many phases.

Relating an equation of state to oxygen fugacity is done using a property called Gibbs free energy. An equation relating how Gibbs free energy varies with temperature and pressure is:

$$dG = -SdT + VdP$$

Where S = entropy
T= temperature
V = molar volume
P = pressure

Therefore, for a fixed temperature: $dG = VdP$
A fundamental property of Gibbs free energy is that when the system is at equilibrium, the G of the products is equal to the G of the reactants. For the tungsten-tungsten oxide system:

$$\frac{x}{2}G_{(O2)} = G_{(WOx)} - G_{(W)}$$

Along the tungsten-tungsten dioxide oxygen fugacity buffer curve, $G_{(O2)}$ is a measured and known quantity at 1 bar of pressure. It takes the equation:

$$G_{(O2)} = RT\ln fO_2$$

The Gibbs free energy of O_2 at higher temperatures and pressures is $G_{(O2)}$ at 1 bar plus the integrated change in Gibbs free energy with respect to pressure. Combining the previous equations, along an isotherm:

$$RT\ln fO_{2(P,T)} = RT\ln fO_{2(1\ bar,\ T)} + \int \Delta V dP$$

Where R = Gas Constant
$\ln fO_2$ = log oxygen fugacity
P = pressure
ΔV = change in molar volume = $V_{oxide} - V_{metal}$

In this final equation, the only unknown term is this ΔV term, or the change in molar volume between the oxide and the metal at temperature and pressure (Campbell et al., 2009). Calculating ΔV allows us to calculate the oxygen fugacity using the previous equation, and plot that oxygen fugacity against temperature to form an oxygen fugacity buffer curve at higher pressures. Buffer curves have been established for tungsten dioxide and tungsten trioxide at 1 bar of pressure (O'Neill et al., 2008), and this research is designed to study how these buffer curves change with pressure. Some research suggests that the valence of tungsten in silicate

melts changes from W^{+6} to W^{+4} as pressure in increased (Cottrell et al., 2009). This would mean we would expect to see the oxygen fugacity buffer curves moving in relation to one another.

Calculating ΔV of tungsten and tungsten oxide at pressure and temperature can be done mathematically if an equation of state is established for each of the phases. To establish these equations of state, we measure how the molar volume of tungsten and tungsten oxide change under different temperature and pressure conditions using x-ray diffraction techniques, and relate the three terms to one equation.

X-ray diffraction is an experimental method wherein a sample is bombarded by a high power x-ray beam, and the x-rays diffract at a given angle based upon the lattice plane with which the x-ray interacts. Assuming the sample crystals are small and scattered in random orientations throughout the sample chamber, it is a safe assumption that all of the varying lattice planes will diffract equally, resulting in a suitable representation of diffraction intensity from of each of the planes. The diffracted x-rays are recorded by a detector that sits behind the sample, and the data appear as a series of concentric diffraction rings surrounding the central x-ray beam. Each diffraction ring represents one 2θ angle at which the x-rays are diffracted and therefore one lattice plane of a phase within the sample chamber. Using Bragg's Law, we can determine the *d*-spacing of a particular lattice plane.

$$n\lambda = 2d(\sin\theta)$$

Where λ = wavelength of x-ray
n = order
d = *d*-spacing

Sometimes, however, lattice planes of different phases within the sample chamber diffract x-rays at the same angle, resulting in overlapping diffraction rings. By collecting multiple diffraction patterns at different temperatures and pressures, we observe how these lattice planes change as a result of the changing temperature and pressure.

High pressures are generated by using a diamond anvil cell, or DAC (Figure 1). The DAC operates by placing faces of two opposing diamonds parallel to one another, and uses screws to squeeze them together. Eventually, the diamond faces meet, and press against each other. Because diamond is such a hard material, it is able to withstand the force pressing against it, but in turn, causes anything between the diamond faces to experience very high pressures. If the sample is placed by itself in between the diamonds it will experience forces and stresses predominately in the direction of the applied force of the diamonds. A metal gasket is placed between the two diamond faces. A hole in the middle of the

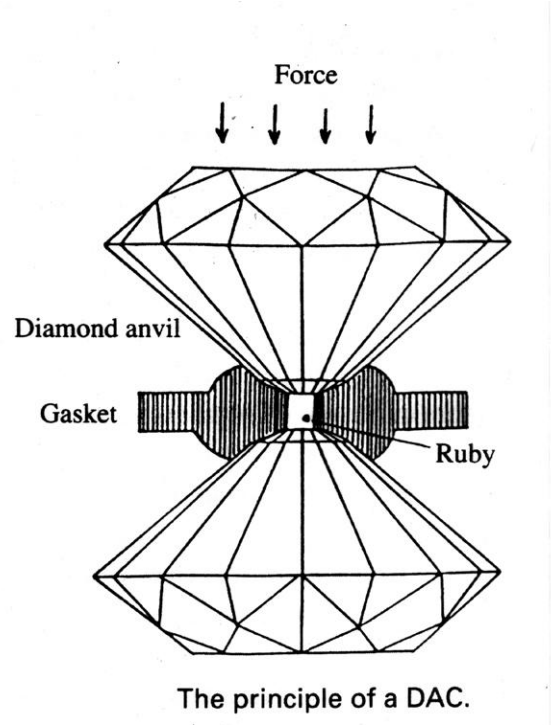

Figure 1. Schematic of a diamond anvil cell (Jacobsen, 2009)

gasket creates a sample chamber, and the metal gasket will become the walls of the sample chamber. In order to accurately describe the properties of the sample phases, phases must experience a hydrostatic environment, meaning that the force of pressure is equal in all directions. A pressure medium is added to the sample chamber along with the sample to create this hydrostatic environment. The pressure medium is able to direct the pressure in a hydrostatic or quasi-hydrostatic manner. In this experiment, we use sodium chloride, NaCl, as the pressure medium. NaCl is a solid and therefore, it does not act like a hydrostatic pressure medium; however, it is very soft so the non-hydrostatic stresses are reduced significantly and at high temperatures produces a much more hydrostatic environment. Pressures and temperatures increase with depth within the Earth, rising up to 100 GPa and 4000 K near the core-mantle boundary.

Using the DAC alone, a number of experiments can be done, all of which are considered "room temperature compression" experiments. These experiments can be useful, but in order to establish a reliable and predictive equation of state, high temperature data must also be collected. The high temperature data in these experiments were collected using a specifically designed heater which works in conjunction with the diamond cell. Developing this heater involved attaching conductive metal wire to a power supply and allowing the electricity to heat the wire. The heater was designed in a way to allow the heat to be conducted evenly throughout the sample chamber.

Designing the heater to work in conjunction with the DAC allowed x-ray diffraction experiments to be conducted through the sample chamber while the sample was experiencing both increased temperature and pressure conditions. Along with the room temperature compression data, the data collected from these experiments were used to establish an equation of state. The x-ray diffraction patterns were analyzed by using a variety of computer programs.

These data are processed using computer software: Microsoft Excel, Fit2D, and Peakfit. 2θ angles are converted into *d*-spacings using Bragg's Law. Joint Committee on Powder Diffraction Standards (JCPDS) cards have been created for a wide variety of materials, and they list the *d*-spacings and the relative intensities of the peak at room temperature and pressure. Changes in the molar volume of each phase can be measured by analyzing the diffraction peaks at different temperatures and pressures. Identifying any possible phase transitions that may occur at increased temperature and pressure is important because phase changes can result in changes to molar volume. Each *d*-spacing peak correlates to a specific set of Miller indices for each phase. These Miller indices are a manifestation of the lattice parameters of each phase. By analyzing many sets of Miller indices, one can determine the specific lattice parameters of each phase, and thus the molar volume of that phase at that specific temperature and pressure. Changing lattice parameters result in changes to molar volume. This changing molar volume is a result of changing temperature and pressure conditions. The relationship among molar volume, temperature and pressure can be expressed for each phase as an equation of state.

These experiments do not require that tungsten react with oxygen, or that tungsten and tungsten oxide remain in equilibrium. There is no available oxygen in the system to react, so unless there is a reaction with a component of the DAC or another phase within the sample chamber, there will be no reaction. We make sure that tungsten and tungsten oxide remain in the same sample chamber, however, to ensure that they are under the same conditions when we measure the ΔV between them. This limits the error in the volume measurements and improves the precision of the experiment as a whole. It is possible to measure tungsten and tungsten oxide

separately, and then apply the calculated volumes to the Gibbs free energy equations, but there are different errors associated with each individual experiment and that could make our calculated ΔV less precise.

3. Geologic Relevance

Understanding the physical and chemical behaviors of all materials that are believed to reside deep within the Earth has become more important as scientists try to understand more about how our planet formed. In order to completely understand all aspects of core formation, it is important to fully understand all of the geochemical properties of the elements that are present in both the core and the silicate Earth, and understand why they are where they are. Along with a number of other elements, tungsten is an element that is partly lithophile and partly siderophile, meaning that it is found in both the core and the silicate Earth. If we are able to better understand some of the chemical properties of tungsten at high temperatures and pressures, we can help to understand how tungsten partitions itself between the silicate Earth and the iron rich core. Similar experiments to measure the effect pressure, temperature, and oxygen fugacity have on metal-silicate partitioning have been conducted for a number of other elements (Rose-Weston et al., 2009; Cotrell et al., 2009; Hillgren et al., 1996; Righter et al., 2003). This can also add to the body of work that is established to determine the specific temperature, pressure, and chemical conditions that were present during core formation of our planet. A discussion by Hillgren et al. (1996) shows fO_2 plays a large role in metal-silicate partition coefficients of some partly siderophile elements.

Also, some scientists use tungsten + tungsten dioxide as a means to control the oxygen fugacity within their experiments. If both tungsten metal and tungsten dioxide are present in a system with available oxygen, and they are at equilibrium with each other, the oxygen fugacity is a known and fixed quantifiable term based on the oxygen fugacity equations. However, if the experiments went to higher temperatures and pressures, the oxygen fugacity may change as a result of the changing external conditions. This change is not well documented or known, and there are suggestions that at higher pressures the valence state of tungsten changes from W^{+6} to W^{+4} (Cottrell et al., 2009). This would cause problems within an experiment because oxygen fugacity is no longer a fixed term.

4. Problem and Hypothesis

I will examine the effects pressure and temperature will have on the oxygen fugacity buffer curves of both tungsten dioxide and tungsten trioxide. Tungsten is an element which exists naturally in different two different valence states: +4 and +6. At high pressure, there is some ambiguity as to which oxide is the dominate oxide which coexists with the pure metal. Some research suggests that at higher pressures, the +4 valence state dominates metal/silicate partitioning (Cottrell et al., 2009), suggesting that the W-WO_2 and the W-WO_3 buffer curves diverge from each other at high pressure. However, my hypothesis is that at higher pressure, the tungsten dioxide and the tungsten trioxide oxygen fugacity buffer curves will move at similar rates with respect to each other.

5. Methods

5.1. Diamond Anvil Cell and Heater

DACs can be used to generate very high pressures similar to those experienced deep within the Earth (Komabayashi et al., 2009). Screws are used to squeeze two parallel faces of opposing diamonds (Figure 2). The metal gasket between the diamonds is indented because of the pressure caused by the diamonds. A hole 80-150 micrometers wide is drilled through the center of the gasket using an electronic drilling machine (EDM). This hole becomes the sample chamber, and the metal gasket becomes the walls of the sample chamber. When the screws are tightened, and the diamonds compress the sample chamber, pressures up to and exceeding 80 GPa can be generated. However, there is no DAC that is able to generate heat in conjunction with pressure, so a heater was developed. A number of different styles of heaters have been developed by other researchers (Komabayashi et al., 2009), and after developing and testing a number of different styles of heaters on our own, one external heater design worked the best. A full discussion of the different designs of heaters can be found in Appendix A.

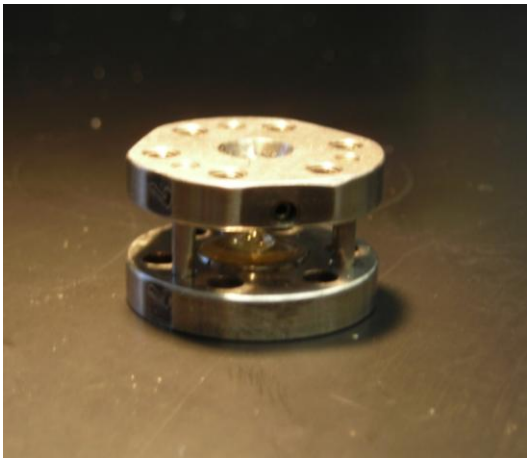

Figure 2. Diamond Anvil Cell. approximately 22mm in diameter and 18 mm tall

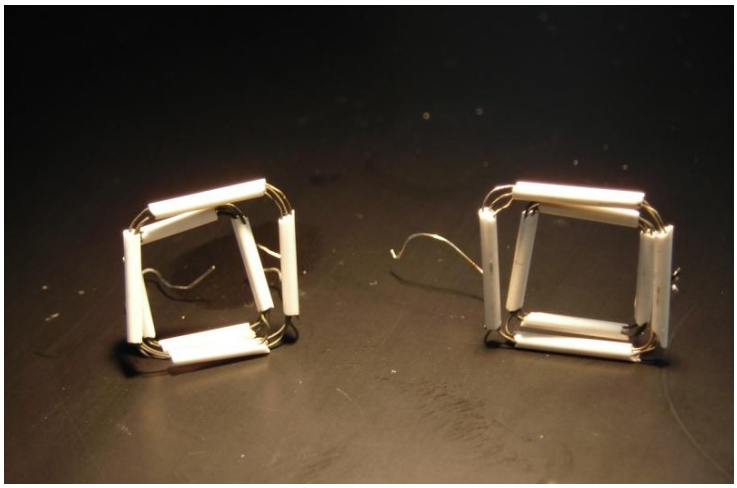

Figure 3. Heater with 4-hole alumina tubing and nichrome wire wound through each hole. Each heater is an approximate square with sides 20mm in length

The final design used nichrome wire wrapped through four-hole alumina tubing as seen in Figure 3, and the tubing was placed outside the two metal plates of the diamond cell. Wire is threaded through each of the 4 holes in a square shape and since this heater is designed to heat the whole DAC there is less restriction on the size of the joints between the tubes. There is space to ensure the wire does not expand and short out the heaters. This also allowed the tubes to be larger in size and more numerous, which allowed more wire to be wound into the system and thus a greater amount of heat. Another advantage to this design is that it allows the temperature gradients throughout the system to be mimized. This more evenly distributes heat throughout the diamond cell, and allows the temperature of the sample chamber to be more accurately measured.

The entire design of the heater revolved around the use of a smaller, more open DAC design (Figure 2) than the diamond cells that are typically used. This design was chosen because it allowed easier thermocouple access to the diamond anvils so the temperature can be accurately measured. However, since this is a less commonly used diamond cell, a new holding block needed to be manufactured to effectively enlarge the size of the DAC so that the center is in a similar location along the x-ray beam line when the x-ray diffraction data are collected. The holding block is made of a pyrophyllite block in the shape of a square with two inch sides (Figure 4). A hole is drilled in the center of

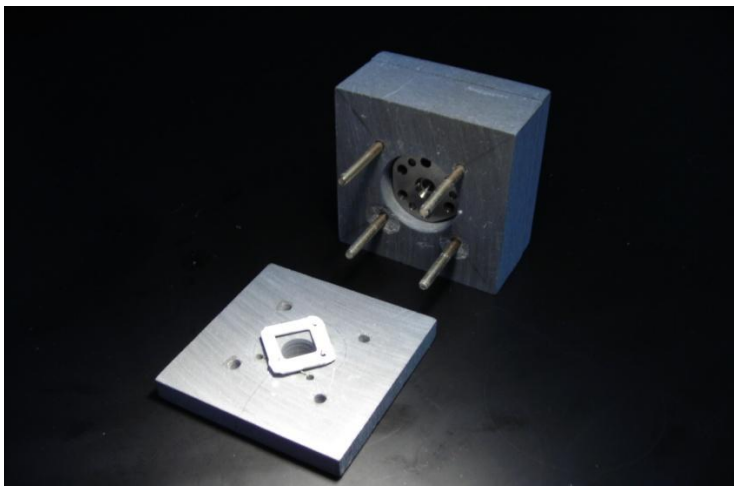

Figure 4. Assembly of diamond cell, insulating block, and heater. Insulating block is made of 2inch square pyrophyllilte.

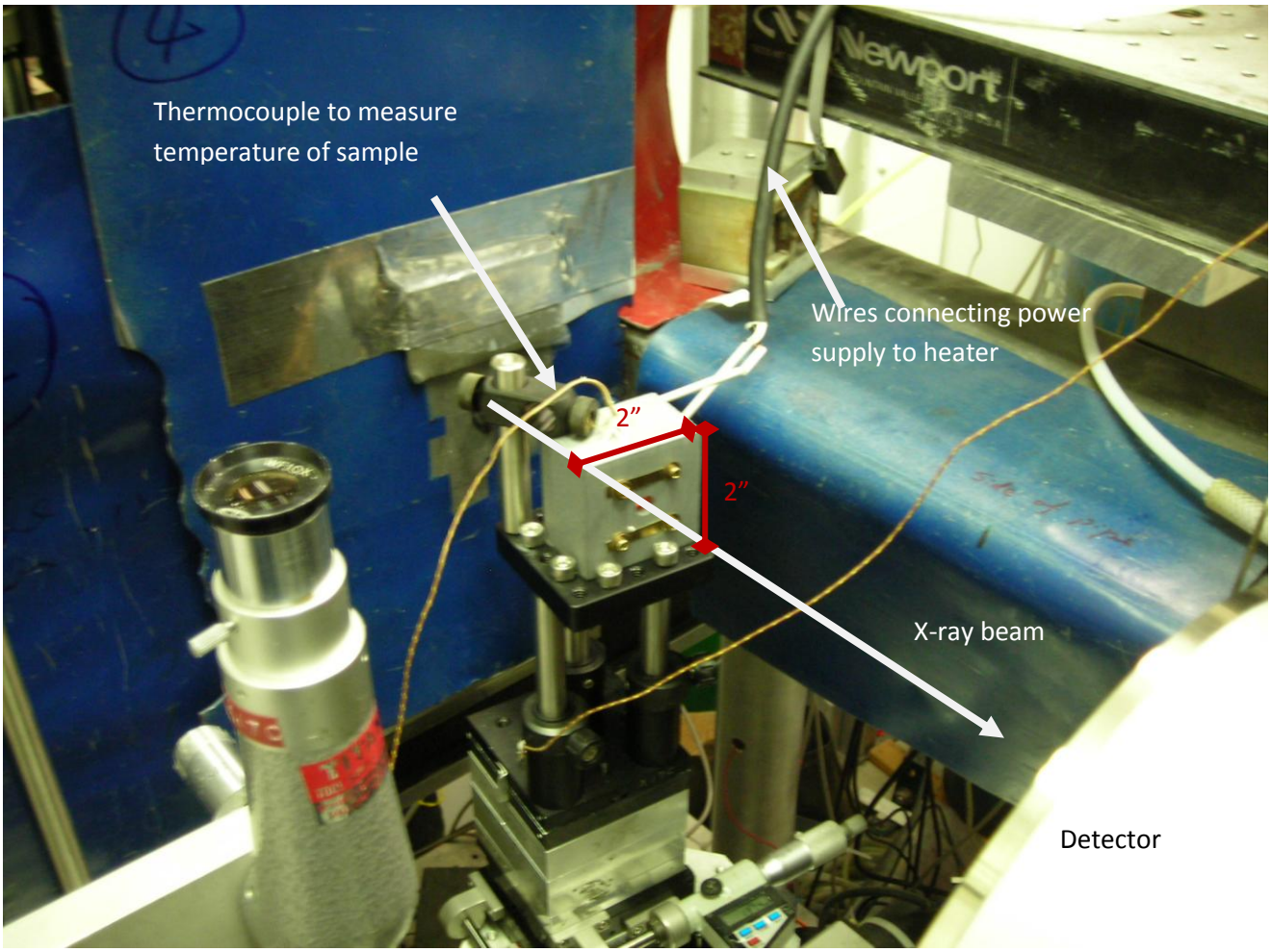

Figure 5. DAC and heater assembly in place along the x-ray beam line at NSLS

the block where the diamond cell sits. Pyrophyllite slabs are placed on each end and everything is held together by screws that travel through the whole block. The screws are attached to both the power supply and the heaters on either end of the diamond cell. Another hole is drilled directly through the center of the top of the block so a thermocouple can travel directly to the sample chamber on the inside and measure the temperature.

5.2.X-ray Diffraction

X-ray diffraction experiments are conducted at the National Synchotron Light Source (NSLS) Beamline X17C at the Brookhaven National Laboratory in Brookhaven, New York (Figure 5). The x-rays are aimed at the sample chamber, and scattered by the material in the chamber and received at a detector which is connected to a computer. An image appears on the computer showing the diffraction rings around the x-ray beam (Figure 6). These diffraction rings are each a different distance around the center x-ray beam, and the distance away from the center of the x-ray beam correlates to a different 2θ angle at which the diffraction occurred. Using computer software (Fit2D), we can turn the diffraction rings into graphs that relate 2θ angle with relative intensity. On these graphs, each peak that is seen corresponds to a ring of a given radius on the diffraction pattern. The sample chamber includes NaCl as a pressure medium, a pressure calibrant (NaCl, Au, or Pt), and the sample materials W and WO_x (Fei et al., 2007). Each material within the sample chamber will diffract the x-rays at different angles based on the crystal structure of the material.

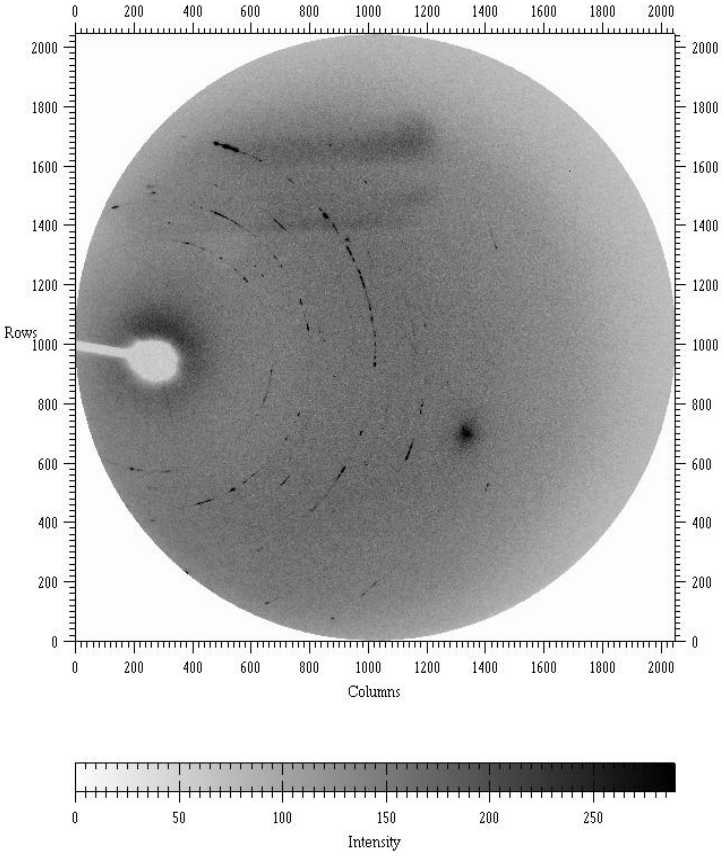

Figure 6 Image of x-ray diffraction scatter pattern collected at NSLS in Brookhaven, New York.

X-ray diffraction patterns are taken while the sample is experiencing different temperature and pressure conditions in order to accurately determine an equation of state at higher temperatures and pressures. This is done by setting the diamond cell to a certain pressure and methodically aligning the cell along the x-ray beam line. A diffraction pattern is then taken at room temperature. The power supply that is controlled by an external source is turned on and the heaters begin raising the temperature of the system. The temperature is raised to 100 degrees Celsius, the sample alignment is verified, and another diffraction pattern is taken. This process continues in increments of 50 to 100°C up to roughly 450° C. Diffraction patterns are taken again as the temperature is brought back to room temperature at similar increments in order to get multiple data points at similar temperature and

pressure conditions to get a measure of precision. When the diamond cell is back to room temperature, it is taken out of the block and the pressure is raised to a moderately higher value. The whole cell is then put back on the x-ray beam line, and the heating cycle process is repeated. The process of heating the cell and taking diffraction patterns is repeated for three cycles, and the temperature – pressure range is thoroughly covered.

5.3. Data Analysis

The x-ray diffraction patterns are taken as images of diffraction rings surrounding the central x-ray beam. This image is input to a program called Fit2-D which turns the image of rings into a graph of intensity vs. two theta angle (Figure 7). The plots are then put into a program called PeakFit which is a program that is able to process the graphs. In PeakFit, the background noise of the images must be removed first in order to make the data relative to one even level. When the background is subtracted, PeakFit picks the largest of the peaks and records their intensity, width, and placement along the two-theta axis. The smaller peaks must be hand picked, and a refinement process built into the program can help to find the precise location, width and intensity of those peaks (Figure 8). When all of the peaks are picked and refined, the program outputs a file with intensity, location, and width of each peak as a numeric file that can be read into Microsoft Excel.

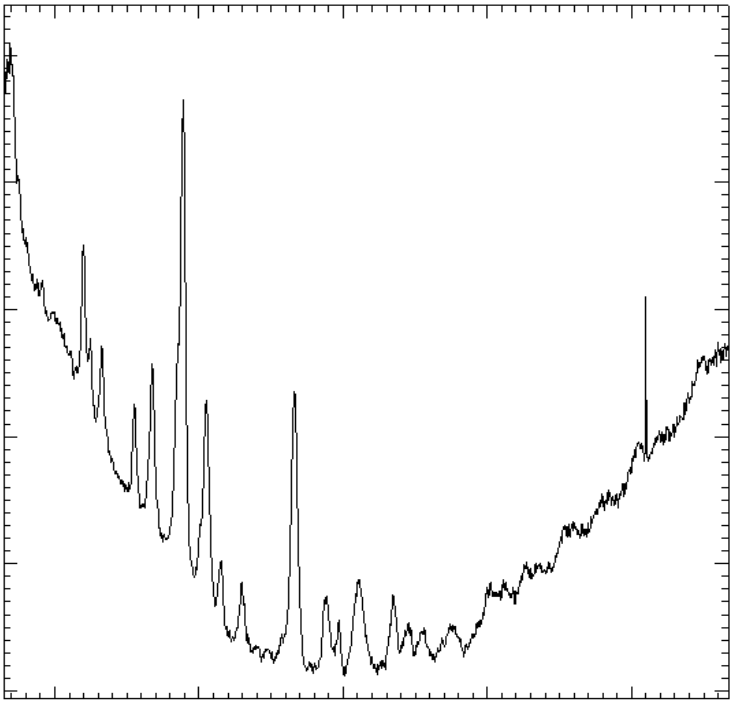

Figure 7. Graph derived from x-ray diffraction scatter pattern plotting relative intensity on the y-axis vs. 2θ angle on the x-axis using Fit2-D

When the data are in Excel, the location as identified as a 2θ angle can be turned into a specific *d*-spacing using Bragg's Law. The *d*-spacing's in each set of data are related to the different phases within the sample chamber. JCPDS cards of the phases tungsten, tungsten dioxide, tungsten trioxide, gold, and sodium chloride give a list of the *d*-spacings of each phase at standard temperature and pressure. The *d*-spacings that are found within the data do not exactly match the *d*-spacings listed in the JCPDS cards because the sample is at high temperature and pressure. Miller indices are assigned to the different *d*-spacings for each phase using help from the JCPDS cards.

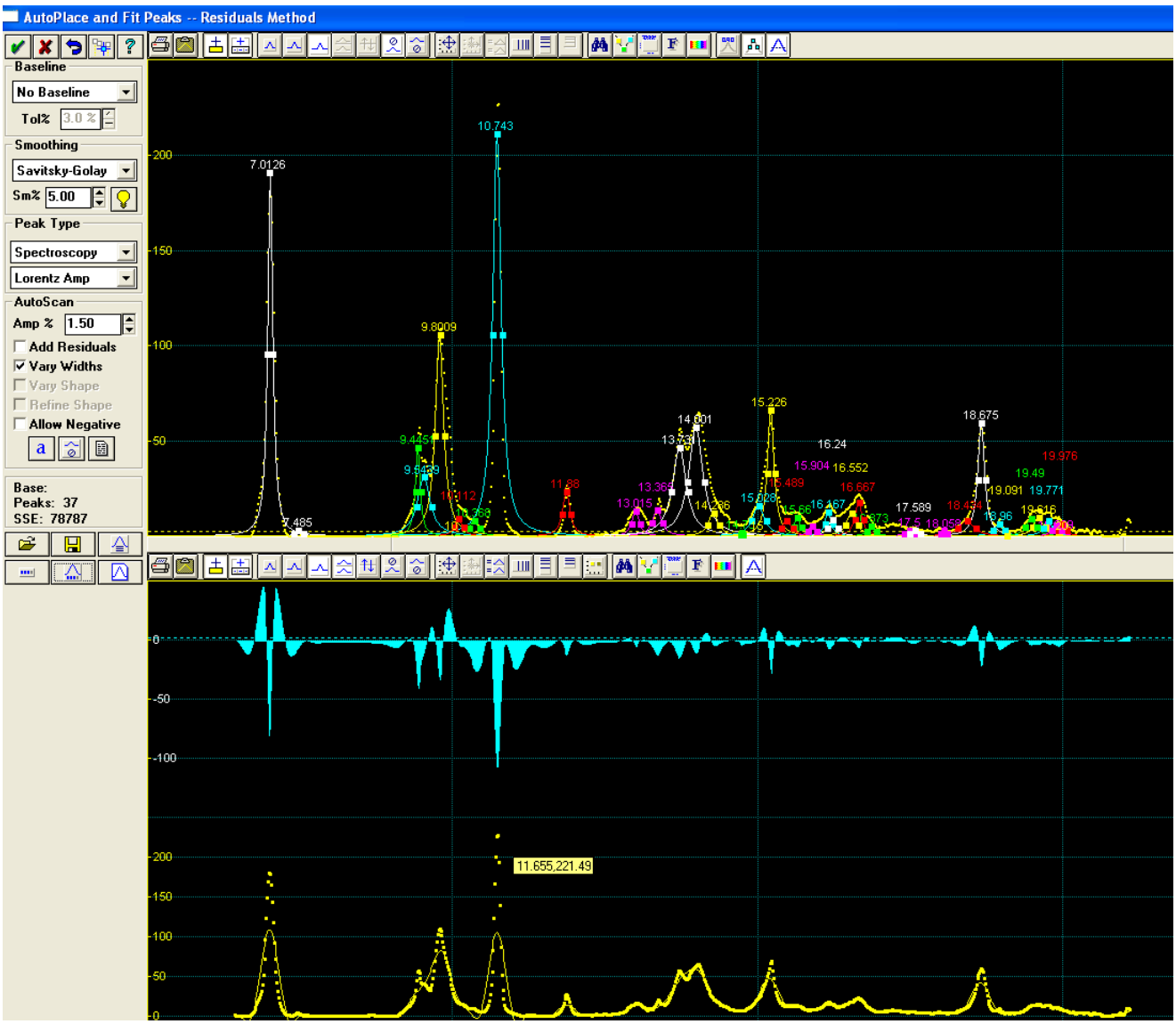

Figure 8. Data analysis using Peakfit program to identify all diffraction peaks

Because the equation of state is very well established for our pressure standard (Fei et al., 2009), we can use the Miller indices and *d*-spacings of these phases to determine the lattice parameters and the molar volume. This molar volume, along with the measured temperature of the system is put into the equation of state for the pressure standard, and a pressure is obtained. This calculated pressure is assumed to be the pressure that the whole sample is experiencing.

Now that both the temperature and pressure of the sample are known, the only remaining parameter that needs to be determined in order to establish an equation of state is the molar volume of the phase. This is done for the tungsten metal and tungsten oxide in a similar fashion as to how it was done for the pressure standard. Using JCPDS cards, Miller indices are assigned to peaks at different *d*-spacings. Tungsten metal, being a cubic system, only has one parameter to determine which is very easy to establish. Tungsten oxide however is known to be monoclinic at lower pressures, and possibly transitioning to orthorhombic at higher pressures. This means that there are four lattice parameters that need to be determined: *a*, *b*, *c*, and β angle. There is no simple equation that can determine all four values, so a solver program is run through Microsoft

Excel to help find them. This is a program that changes all four values simultaneously while trying to minimize the difference between the measured *d*-spacings and the calculated *d*-spacings that would result from the given lattice parameters. Knowing all four lattice parameters gives the ability to determine the third component of the equation of state the tungsten oxide: molar volume.

The uncertainties within this experiment will come from the lattice parameters that are calculated from the diffraction patterns. When the data are processed in the Excel spreadsheet, it instantly becomes clear that the calculated lattice parameters are not always going to match each other. For instance, the assigned Miller indices for tungsten metal should all give 1 calculated lattice parameter because tungsten has a cubic structure, and only 1 lattice parameter is needed to describe cubic systems. For cubic systems, the lattice parameter is calculated by the equation:

$$a = d\,(\sqrt{(h^2+k^2+l^2)})$$

Where a = lattice parameter
d = measured *d*-spacing
h,k,l= set of Miller indices

However, the calculated lattice parameter does not result in *d*-spacings of the exact same value as the measured *d*-spacings. The difference between the calculated lattice parameters and the measured lattice parameters determines the error in the measurements, and that error is then propagated through the equation that relates the calculated lattice parameters into calculated volumes, and further propagated through into the equation of state. For the tungsten oxide however, calculating the lattice parameters is not as easy because the system is monoclinic, but the same principles apply. A solver program in Microsoft Excel calculates what the *d*-spacing should be based on assumed lattice parameters. The program changes the assumed lattice parameters until the calculated *d*-spacings are as close as possible to the actual measured *d*-spacings. It is this difference in calculated *d*-spacing compared to measured *d*-spacing that is used to measure the error for the tungsten oxide. Similarly, this error is also propagated through the volume calculation and into the equation of state. Errors in volume for both the tungsten metal and the tungsten dioxide are on the order of 0.2%.

5.4. Equation of State

The Birch-Murnaghan equation of state (Fei et al., 2007) is described as:

$$P(V) = 3K_0/2\,[(V_0/V)^{7/3} - (V_0/V)^{5/3}]\{1+3/4(K_0' - 4)[\,(V_0/V)^{2/3} - 1]\}$$

Where: P= pressure
V= Measured volume
V_0= Volume at standard temperature and pressure
K_0= Bulk modulus = $-V(\partial P/\partial V)_T$
K_0'= Bulk modulus pressure derivative

The bulk modulus is essentially the compressibility of a material. The lower the bulk modulus, the easier that material is to compress. Likewise, the bulk modulus pressure derivative is a measure of how the bulk modulus changes as the pressure is increased. The bulk modulus and its pressure derivative are quantities that have been previously determined using room temperature compression experiments (Shofner et al., in preparation), and are quantities that are properties of the material, in this case tungsten and tungsten oxide, that we assume to be fixed values.

5.5. Oxygen Fugacity Calculation

The equation of state is used to determine the pressure effect on oxygen fugacity for both tungsten dioxide and tungsten trioxide. The equation of state relates molar volume to temperature and pressure, and it is this relationship that is needed to determine pressure effect on oxygen fugacity. Using the oxygen fugacity equation described earlier, R, T, and $\ln fO_{2\,(1bar,T)}$ are all terms that are either known or have been developed during previous research, and $\ln fO_{2\,(P,T)}$ is the term we are trying to establish. The only other unknown term in this equation is the ΔV term, relating the molar volumes of the metal and the oxide. This ΔV term will be determined through the equations of state for each of the phases. Using this equation of state, for any pressure and temperature we can calculate the molar volume of each phase and calculate the difference between them. Then we apply that molar volume difference to this oxygen fugacity equation and calculate how the oxygen fugacity changes with respect to temperature and pressure (Campbell et al., 2009). These changes are more easily seen visually on a graph. Oxygen fugacity is plotted versus temperature, and the curve that appears is called a buffer curve (Figure 9).

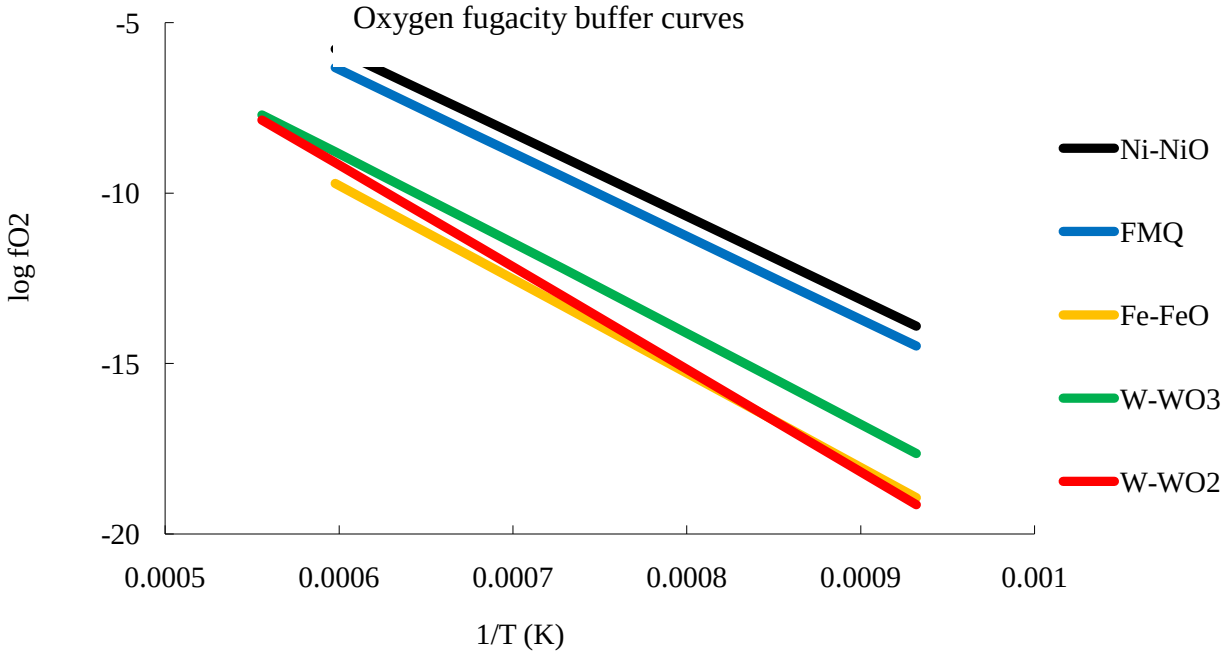

Figure 9. Oxygen fugacity buffer curves for W-WO_2 and W-WO_3 in relation to other known buffer curves at 1 bar of pressure (Campbell et al., 2009; O'Neill et al., 2008)

6. WO_2

6.1. Equation of State Analysis

We subjected the WO_2 powder to elevated temperature and pressure conditions up to 700 Kelvin and 45 GPa and performed x-ray diffraction experiments to observe how the materials volume changed as the conditions were changed by the methods described earlier. The WO_2 crystal structure behaved by shrinking as the pressure increased while expanding as the temperature was raised, as expected. Using the processed x-ray diffraction data and Microsoft Excel, I indexed the diffraction peaks according to JCPDS cards, allowing me to plot the changes in lattice parameter with pressure (Figure 10).

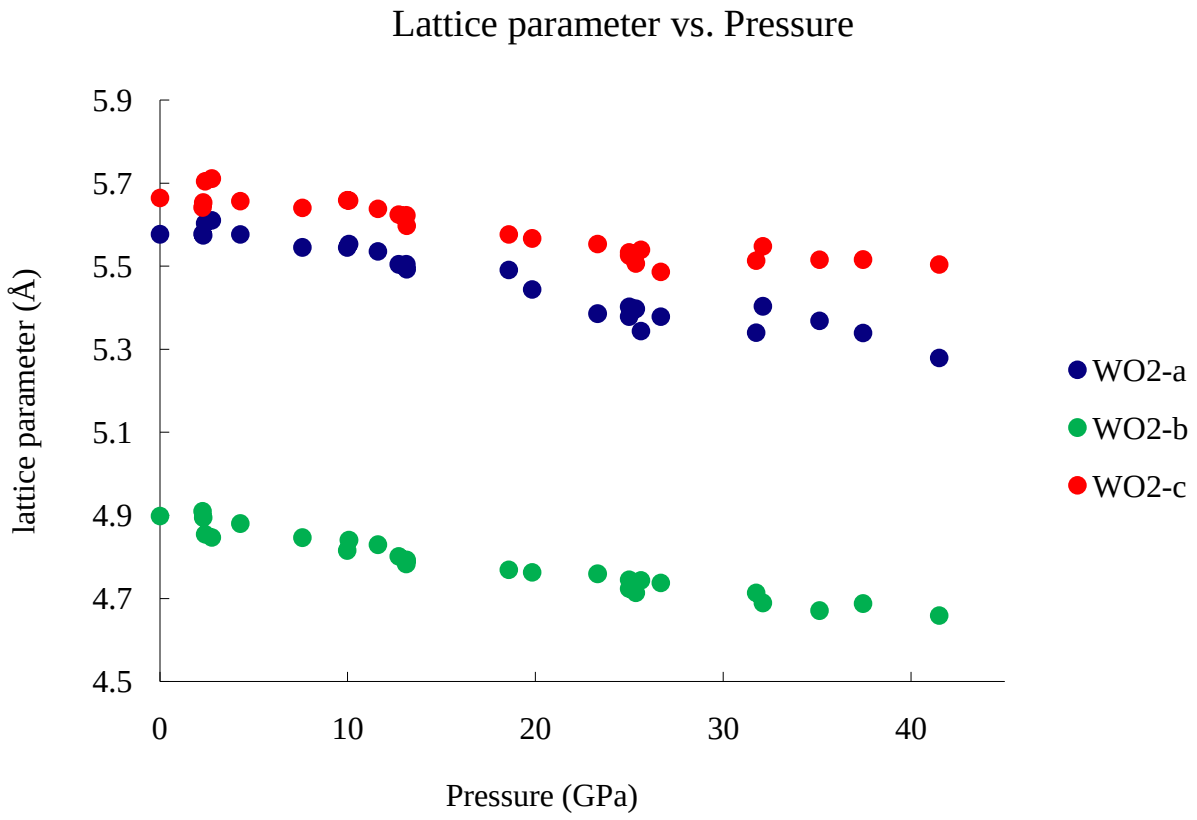

Figure 10. Plot showing WO_2 lattice parameters vs. pressure

These a, b, and c lattice parameters trend in similar directions and at similar slopes to one another as the pressure is increased. The calculated molar volumes derived from the lattice parameters each have associated temperature and pressure conditions under which they were formed. To determine this relationship I create an F vs. f plot of all my data using the Birch-Murnaghan equation of state found in section 5.4, where after rearranging:

$f = \frac{1}{2}[(V/V_0)^{-2/3} - 1]$ = negative eulerian strain

$F = K_0 + 3/2K_0(K_0' - 4)f$

This relationship takes the form of a linear equation where the y-intercept is the bulk modulus K_0 and the slope is set equal to $[3/2K_0(K_0' -4)]$ to determine K_0'. A negative slope of the trend line suggests a K_0' value less than 4, where as a positive slope suggests a value greater than 4. If the data points seem to be along one horizontal line, which is the case for a wide variety of materials, K_0' is inferred to be 4.0.

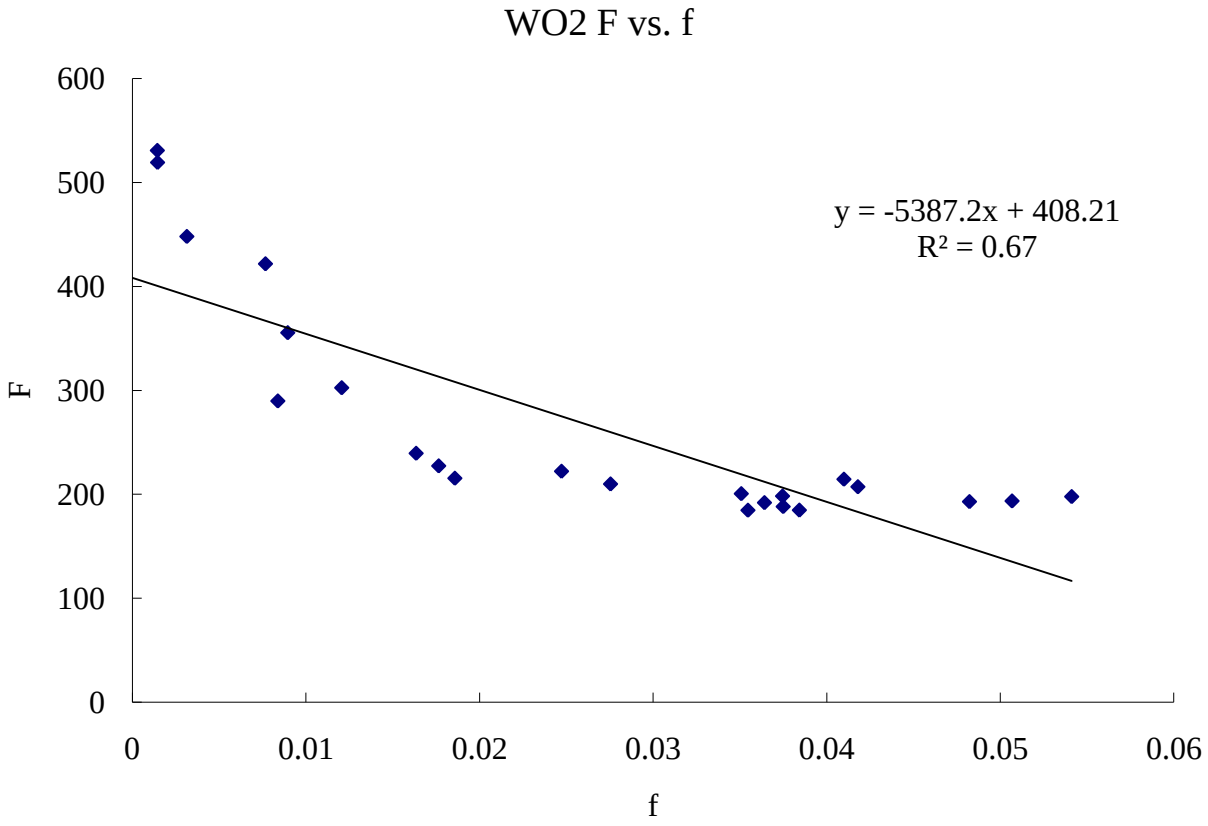

Figure 11. F vs. f plot of WO_2 data, showing a distinct bias in the low-f data

While 2/3 of the data on the "high-f" portion of the graph in Figure 11 seem to follow this quasi-horizontal line pattern, there is a significant and consistent upswing on the low-f side of the graph, which is a consequence of the data being measured at different temperatures and not isothermally. Therefore, we decided to change the method of determining K_0 and K_0'. We assume K_0' to be 4, simplifying the second half of the Birch-Murnaghan equation of state and determining the temperature component of the equation of state by assuming

$$P_{total} = P_{300} + (\partial P/\partial T)_V(\Delta T)$$

Where: P_{300} = Burch-Murnaghan equation of state

dP/dT = change in pressure with respect to temperature, simple temperature correction

Rearranging this equation and inserting the Burch-Murnaghan equation of state we find:

$$P/\Delta T = 3K_0f(1+2f)^{5/2}/\Delta T + (\partial P/\partial T)_V$$

Again, we have the form of a linear equation if we plot $[3f(1+2f)^{5/2}/\Delta T]$ vs. $[P/\Delta T]$ where K_0 becomes the slope of the trendline and $(\partial P/\partial T)_V$ is the y-intercept.

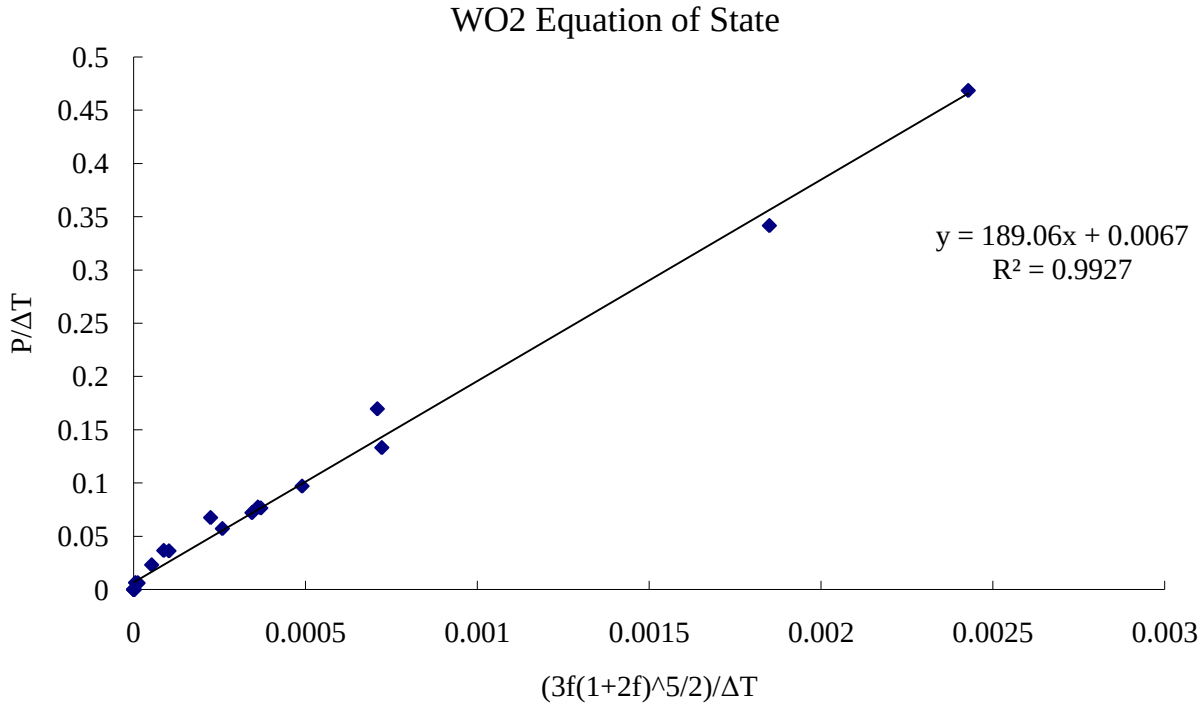

Figure12. Plot used to determine the equation of state for WO_2

Clearly, this graph in Figure 12 fits the data much better as shown by the R^2 value. This results in a pressure and temperature dependent equation of state for WO_2 with $K_0 = 189.06$, $K_0' = 4.0$, and $(\partial P/\partial T)_V = .0067$

$$P = 3(189.06)f(1+2f)^{5/2} + .0067\Delta T$$

6.2. WO_2 oxygen fugacity calculation

The calculation for oxygen fugacity for WO_2 is solely dependent upon the development of its equation of state. Now that I have established this equation of state, I calculate the equation of state using SCILAB routines that have been previously designed and used and proven to work effectively (Campbell et al., 2009). The oxygen fugacity equations:

$$RT\ln fO_{2(P,T)} = RT\ln fO_{2(1\ bar,\ T)} + \int \Delta V dP$$

Where R = Gas Constant

$\ln fO_2$ = log oxygen fugacity

P = pressure

ΔV = change in molar volume = $V_{oxide} - V_{metal}$

Again, the only unknown on the right side of this equation is the ΔV term integrated with respect to pressure, and this is known once the relationship between the two is determined. I modify the preexisting scilab files by first inserting the new K_0, K_0', and dP/dT terms and modifying the 1bar oxygen fugacity equation according to the equation given for the W-WO_2 buffer curve by O'Neill, et al., 2008. I also needed to modify how the temperature term is calculated because in the previous experiments by Campbell et al. the scilab routines used a more sophisticated temperature term in the equation of state. I wanted the simple [$P_{total} = P_{300} + dP/dT(\Delta T)$], where the temperature term is controlled solely by dP/dT.

Modifying the form of the equation of state and importing the newly acquired WO_2 data, I was able to determine the oxygen fugacity at each temperature point, and plot how this oxygen fugacity curve moves with increasing pressure (Figure 13).

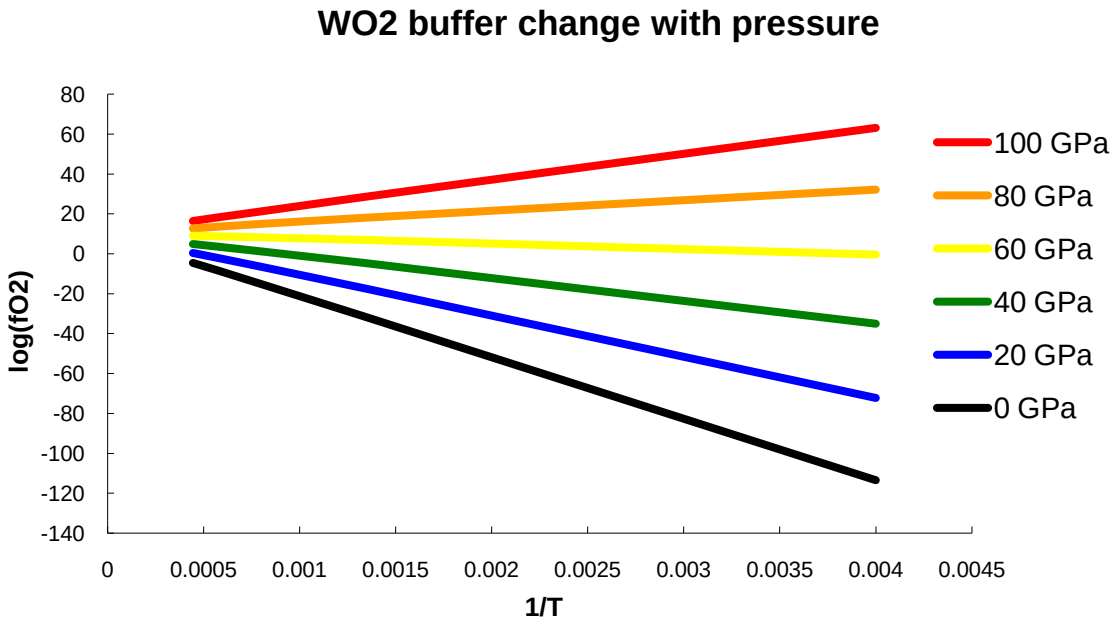

Figure13. WO_2 oxygen fugacity buffer curve with changing pressure.

7. WO_3

7.1. Equation of State Analysis

We determined the equation of state for WO_3 in a different manner than the WO_2 because we collected room temperature compression data, and not high temperature data. These data gave us the ability to calculate K_0 and K_0' for the species, but not the temperature term. The first and most glaring aspect of WO_3 that I came across showed that WO_3 had many stable phases depending upon the temperature and pressure conditions. At room temperature and pressure conditions there are at least three stable phases of the species, and as conditions are changed the phases change an unknown number of times. Bouvier et al. (2002) did similar room temperature compression experiments with WO_3 and discovered a similar situation. They were able to recognize 3 different phase changes. Above 0.15 GPa, a monoclinic ε-phase is present. Above 0.57 GPa, a different monoclinic phase ($P2_1/c$ space group) is stable. This phase is stable up to 22 GPa, where another monoclinic phase ($P2_1/a$ space group) is stable. Above 31 GPa a space

group Pm monoclinic phase is stable (Bouvier et al., 2002). Bouvier et al. (2002) gave calculated lattice parameters and initial volumes for each of the phases at high pressures. I was able to use their calculated lattice parameters as a base for my data, index my diffraction patterns accordingly, and calculate volumes similar to Bouvier's data with low errors.

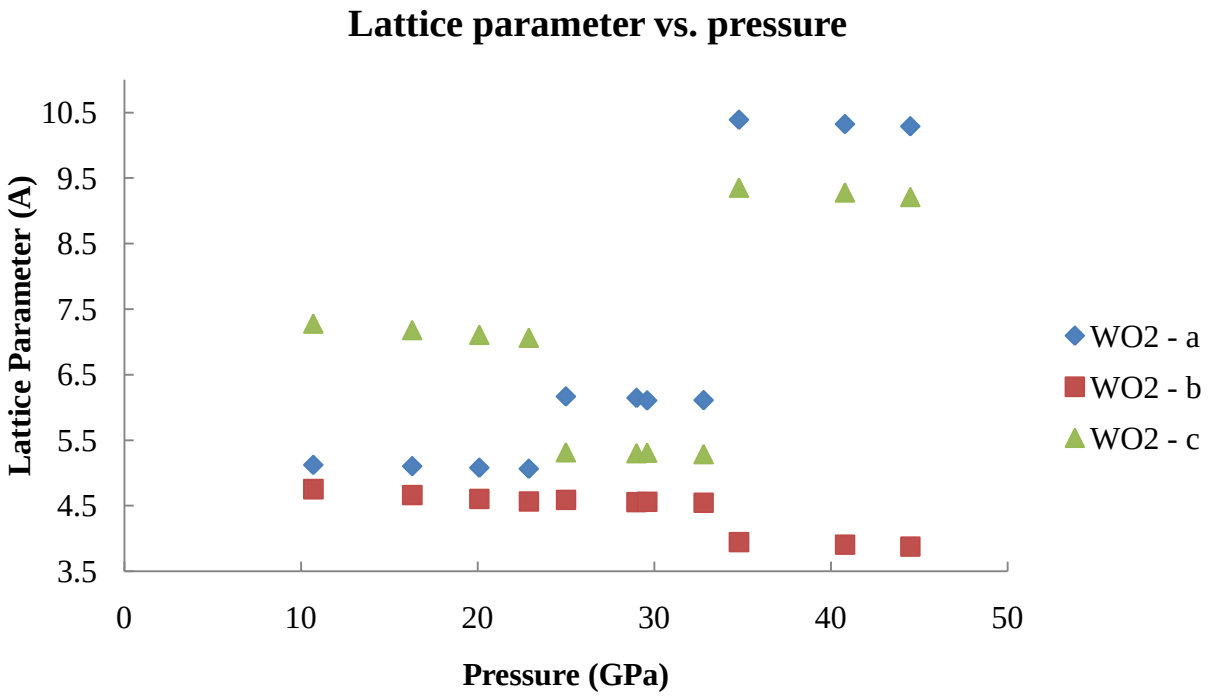

Figure14. Lattice parameter plotted against pressure for the indexed WO_3 diffraction patterns

Looking at the data points in Figure 14 above 10 GPa, we see that there are three distinctly different phases with very different lattice parameters, however they are internally consistent with similar slopes as the pressure is raised and they match the data given by Bouvier et al.

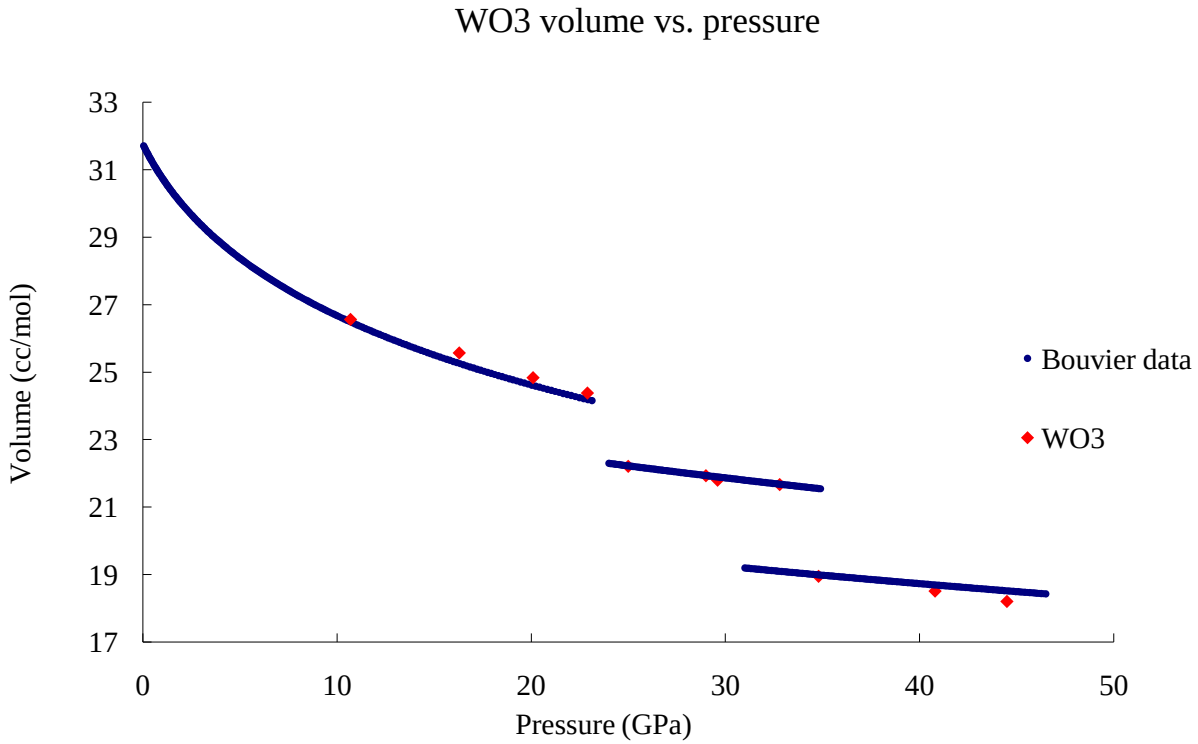

Figure15. WO_3 volume plotted against pressure for indexed WO_3 data as well as isothermal compression curve derived from Bouvier

By using the K_0 and K_0' values derived by Bouvier for each of the species, I created an isothermal compression curve for the individual species and plotted my data against the compression curves (Figure 15). My data agree fairly well with the previously recorded data.

One major issue with the compression data of Bouvier et al. (2002) comes from Dorogokupets and Oganov (2007) who identify an error in the pressure calibration used by Bouvier. Bouvier used a method called ruby fluorescence to determine pressures within the DAC: the R_1 line shift of ruby luminescence is calibrated to changes in pressure according to the equation

$$P = A/B[(\lambda/\lambda_0)^B - 1]$$

Where:

P = pressure

$A = \lambda(\delta P/\delta\lambda) = 1904$ GPa

$B = 7.665$

$\lambda_0 = 694.24$ nm (Mao et al., 1986)

Dorogokupets and Oganov (2007) found that Mao's ruby fluorescence calibration did not fit other means of calculating pressure, especially at higher pressures. Up until roughly 45 GPa, Mao's calibration resulted in a pressure about 0.75-1 GPa lower than other calculated pressures and after 45 GPa, the calibration gives progressively lower pressure values until roughly 130 GPa where the pressure calibration is 10 GPa shy of other calibrations. I was able to back-calculate Bouvier's measured λ values using Mao's original equation, and apply the raw λ into Dorogokupets and Oganov's new calibration equation to obtain corrected pressures for Bouvier's data (Figure 14).

$$P = 1884 * (\Delta\lambda/\lambda_0)*(1+5.5(\Delta\lambda/\lambda_0))$$

Bouvier P	Pcorrected	Bouvier P	Pcorrected	Bouvier P	Pcorrected
1.060	1.051	**7.390**	7.376	**16.270**	16.383
1.560	1.547	**8.050**	8.040	**17.230**	17.365
2.310	2.293	**8.830**	8.826	**18.040**	18.196
3.270	3.249	**9.260**	9.260	**19.250**	19.438
3.990	3.968	**10.090**	10.098	**19.940**	20.147
3.460	3.439	**11.110**	11.131	**20.870**	21.105
4.000	3.978	**11.690**	11.719	**21.820**	22.084
4.800	4.777	**12.470**	12.510	**22.200**	22.477
5.690	5.669	**13.360**	13.415	**23.060**	23.365
6.380	6.361	**13.900**	13.965		
6.840	6.823	**15.420**	15.514		

Figure16. Data table of pressure correction of Bouvier's data up to 23 GPa

I performed the pressure correction to Bouvier et al.'s data and using a combination of their data and my data re-ran the calculations to determine the new equation of state parameters K_0 and K_0'. I combined the data because he had much more data points than I did and my data matched with his data reasonably well.

To calculate a full equation of state that relates volume to temperature and pressure, I need data on WO_3 as a function of changing temperature. Howard et al. (2001) performed very high-resolution neutron powder diffraction experiments on WO_3 at 1bar of pressure from room temperature up to 1000 ^oC. At room temperature they found a monoclinic space group $P2_1/n$. From 350 – 720 ^oC an orthorhombic space group Pbcn was observed. From 720 – 800 ^oC they found a monoclinic $P2_1/c$ space group and from 800 to 900 ^oC a tetragonal structure in space group P4/ncc, and above 900 ^oC a second tetragonal structure in P4/nmm.

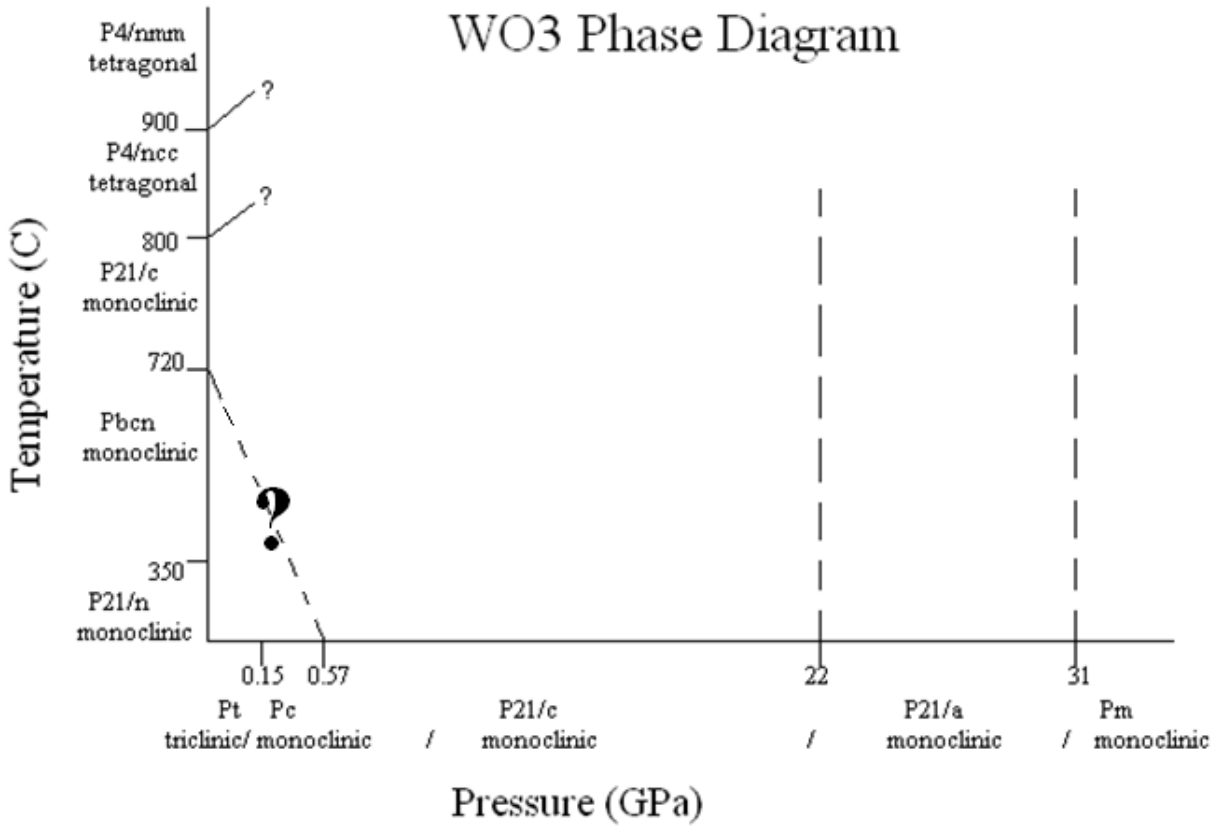

Figure17. Phase diagram for WO_3 based on data collected from Bouvier et al. (2002) and Howard et al. (2001)

Using the data proposed by Bouvier et al. and Howard et al. we can construct a pressure-temperature phase diagram for WO_3 (Figure 17). We notice that both research teams found a $P2_1/c$ monoclinic space group within their data. We can also determine the sign of the Clapeyron slope for the species along the temperature axis based on the known volume change of the transitions and the fact that the higher temperature phases must have higher entropies. There is no temperature data on the high pressure phases, so I can only assume vertical lines for the phase boundaries, and the Clapeyron slope is positive for the high temperature phases. The Clapeyron slope at 720 ^oC is negative. Howard et al. gives lattice parameters for this phase at 760 ^oC: a = 5.2793 Å, b = 5.2635 Å, c = 7.8329 Å, $\beta = 90.483^o$. Bouvier et al. (2002) give lattice parameters at 1.06 GPa of a = 5.2557 Å, b = 5.0986 Å, c = 7.6242 Å and $\beta = 92.169^o$. Because both groups found the same space group in their studies, the lattice parameters of these species are similar, the molar volumes of these species are similar, and the Clapeyron slope would be in the correct (negative) direction, I am assuming that these two species are in fact one in the same. I am assuming only 1 monoclinic $P2_1/c$ space group phase, and the space connecting the two axes is filled with this one phase. The original motivation behind this research involved finding a reasoning behind the statement by Cottrell et al. that at high pressures the WO species switches

from WO_3 to WO_2, and her experimental conditions were in the vicinity of 15 GPa, I am only going to concern my research with the $P2_1/c$ monoclinic space group of WO_3 which occupies that portion of the phase diagram.

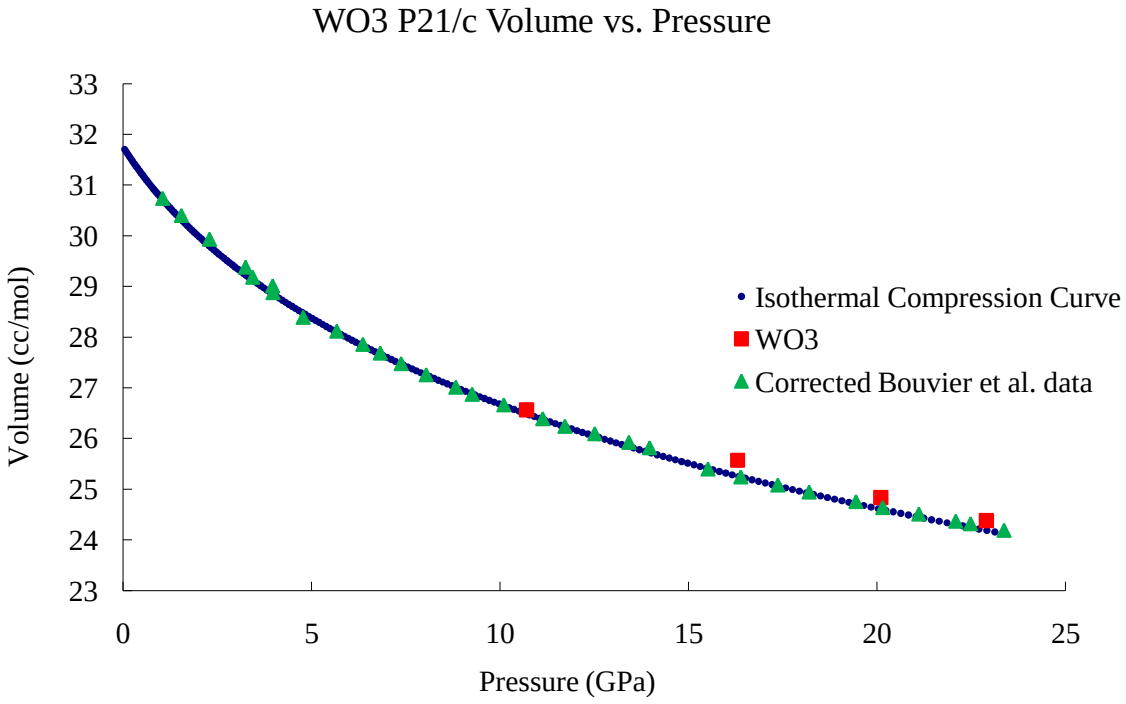

Figure 18. WO_3 space group $P2_1/c$ data plotted against the corrected Bouvier data and the corrected isothermal compression curve

I determine K_0 and K_0'of WO_3 using the corrected room temperature compression data from Bouvier et al. in combination with my collected data (Figure 18).

$K_0 = 28.2$ GPa

$K_0' = 9.1$

By combining these values with the data of the same phase from Howard et al. we can determine the temperature component of the equation of state for this particular phase. Howard et al. give data of molar volume as a function of temperature for each phase. We know that

$$\alpha = (1/V)*(\partial V/\partial T)_P$$

We can take an average of the molar volume over the $P2_1/c$ temperature span and that can be our representative V. By measuring the average slope of that section of the graph we can determine dV/dT.

$V = (54.6125+54.26775)/2 = 54.4401$

$(\partial V/\partial T)_P = (54.6125-54.26775)/(790-730) = 0.005746$

$\alpha = 1.055 \times 10^{-4}$

Usint the same equation of state form that I used for WO_2:

$(\partial P/\partial T)_v \approx \alpha K_0$

$(\partial P/\partial T)_v = .00297 \times 10^{-3}$

The equation of state for WO_3 space group $P2_1/c$ is therefore:

$P = 3(28.2)f(1+2f)^{5/2}[1+3/2(9.1-4)f] + .00297\Delta T$

7.2. Oxygen Fugacity calculation

The same oxygen fugacity calculations that were applied to WO_2 within the Scilab routines were also applied using the WO_3 equation of state, with the only difference being the 1 bar oxygen fugacity equation given by O'Neill et al. (2008). Applying the changes to the equation of state and 1 bar oxygen fugacity equation allowed me to plot an oxygen fugacity buffer curve at different pressures for WO_3, space group $P2_1/c$ (Figure 19).

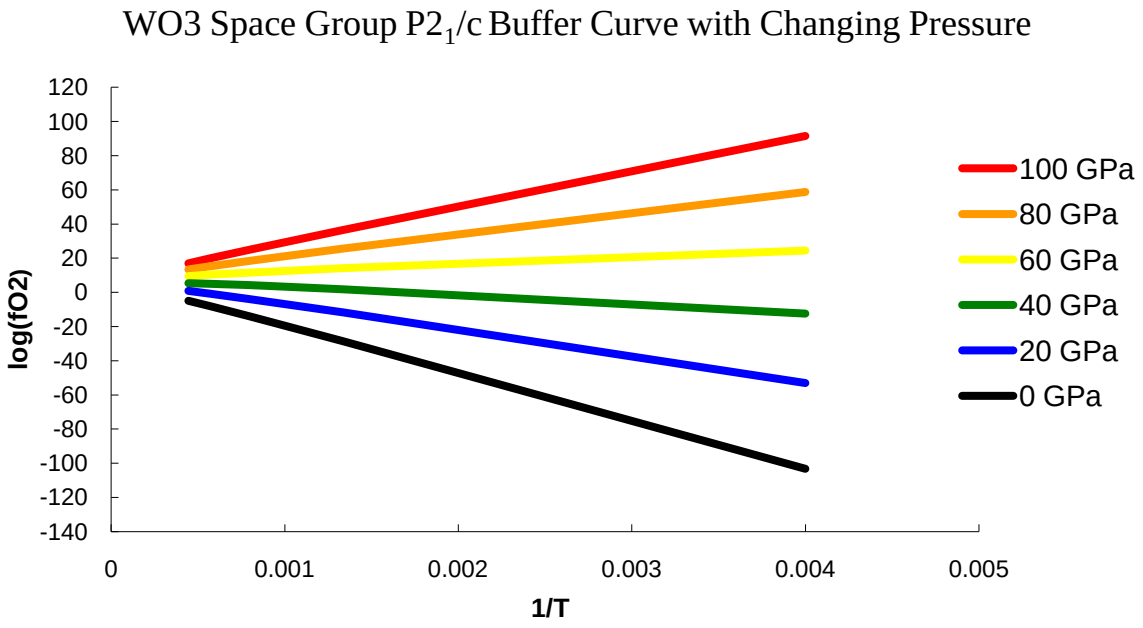

Figure19. WO_3 space group $P2_1/c$ buffer curve plotted for changing pressure

8. Buffer Curve Comparison

By looking at Figures 13 and 19 individually, it is very difficult to determine if there are any discrepancies or differences between them. The original question asked how these two buffer curves changed with respect to one another as the pressure was increased. The easiest way to observe the changes between them is to plot them on the same diagram.

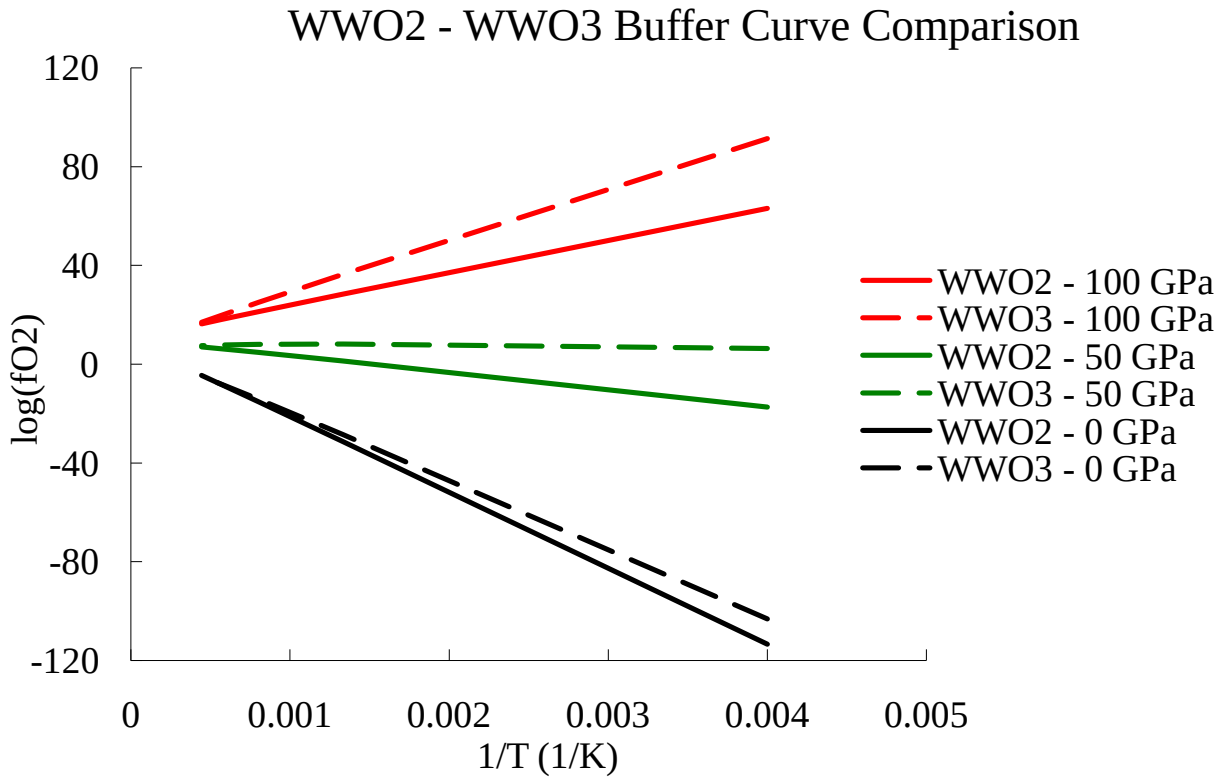

Figure20. WO_2 and WO_3 buffer curve comparison with increasing pressure

Figure 20 shows that as the pressure is increased, the WO_3 buffer curve is increasing its slope at a faster rate than the WO_2 buffer curve. By looking at where 1/T = .004 (T = 250K) we see that the log(fO2) difference between WO_3 and WO_2:

$WO_3(\log(fO_2)) - WO_2(\log(fO_2)) = \Delta\log(fO_2)$

@ 0GPa : (-103.1764) - (-113.4556) = 10.2792

@ 50 GPa: 6.3600 - (-17.4174) = 23.7774

@ 100 GPa: 91.4465 - 63.1657 = 28.2808

As we can see, increasing the pressure increases the distance between the two buffer curves, meaning that the WO_3 buffer curve is moving upwards at a faster rate than the WO_2 curve.

9. Summary/ Discussion

In order to fully understand how and why the Earth differentiated into the iron rich core and the silicate portions of the Earth, we must understand how elements partition between the two. By establishing an equation of state for tungsten dioxide and tungsten trioxide I can analyze the oxygen fugacity relationship between the two buffers at high pressure. The oxygen fugacity relationship can help to determine whether W^{+4} or W^{+6} is more prevalent at high pressures deep within the Earth, and add to the body of work that is compiled to better understand the conditions that were present during core formation.

Establishing this equation of state was done using a diamond anvil cell, an external heater, and x-ray diffraction techniques. I placed tungsten metal and tungsten oxide in the DAC to apply pressure, heated the sample, and measured how the molar volume changed as a result. The equation of state was related to Gibbs free energy and ultimately oxygen fugacity. $Log(fO_2)$ is plotted against temperature to create an oxygen fugacity buffer curve for both tungsten dioxide and tungsten trioxide, and these curves are analyzed with respect to each other at high pressure to help to understand how the two materials behave. My hypothesis was that the two buffer curves move similarly with respect to each other as the pressure is increased.

Ultimately, my hypothesis was incorrect. The two buffer curves both moved upwards on the oxygen fugacity plots, but they moved at different rates from one another. The WO_3 buffer curved changed its slope at a faster rate than the WO_2 buffer curve. This actually is a phenomenon that would seem to make sense given the results of Cottrell et al. They stated that they observed WO_2 becoming more prevalent within silicate melts as they traveled deeper within the Earth, meaning that at higher temperature and pressure conditions the WO_2 phase was becoming more stable.

By looking at Figure 20, we see that the WO_2 buffer curve is below the WO_3 buffer curve, even at 0 GPa. This means the WO_2 phase would have a lower Gibbs free energy than the WO_3 phase, making WO_2 more stable even at 0 GPa. The increasing distance between the two curves as pressure is increased suggests that at higher pressure, WO_3 is constantly increasing its ΔGibbs free energy with relation to WO_2, making WO_2 increasingly more stable as the pressure is increased, just as Cottrell et al. stated. The only remaining question would be that if at 0 GPa WO_2 had a lower Gibbs free energy than WO_3, why is WO_2 not the stable phase present in silicate melts at low pressure – and the answer must reside in their activity coefficients.

Appendix A.

The original heater design involved creating an internal heater out of an insulating pyrophyllite disc by drilling pairs of holes through the pyrophyllite from top to bottom. The entire disc then has a hole drilled through the middle, big enough so the heater can sit around the diamonds and the sample chamber of the diamond cell. This would create one ring of holes through the disc at a small radius, and another ring of holes through the disc at a larger radius on the disc (Figure 21). Nichrome wire would then be thread through the outside pairs of holes and connected to a power supply. When the power supply is turned on, electricity would run through the bare wire, causing it to heat up. The heat would be conducted through the insulating pyrophyllite disc, and into the sample chamber causing the sample chamber to heat up.

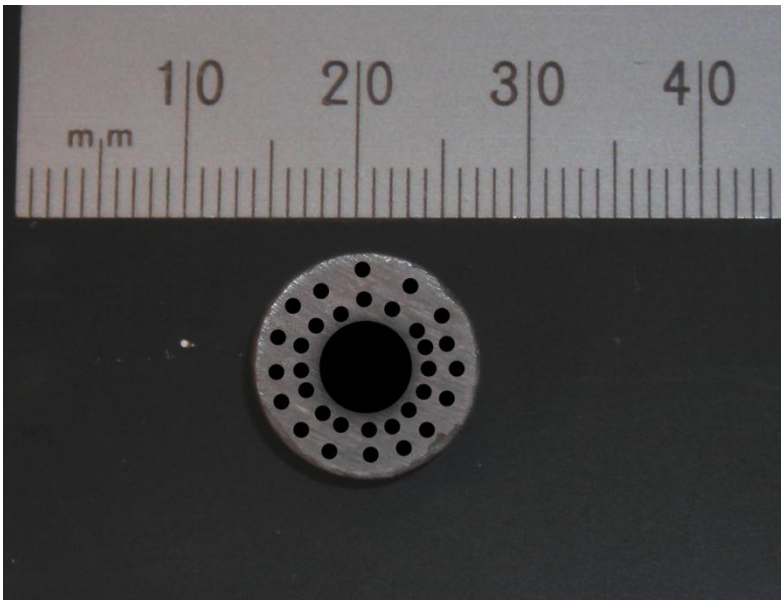

Figure 21. First heater design. Central hole for the sample chamber surrounded by wire threaded through holes in pyrophyllite cylinder. Holes simulated because pyrophyllite would break during machining

However, this design had flaws. This design did not allow for any thermocouple to be inserted into the sample chamber, so there would be no way of accurately measuring the temperature of the sample. Drilling the small holes for the heater wire to be thread through caused the block to break apart very easily. Pyrophyllite is not a particularly strong material, and the stress of drilling so many small holes in such a small area caused it to break down. The manufacturing of this heater ended up being the downfall of this design.

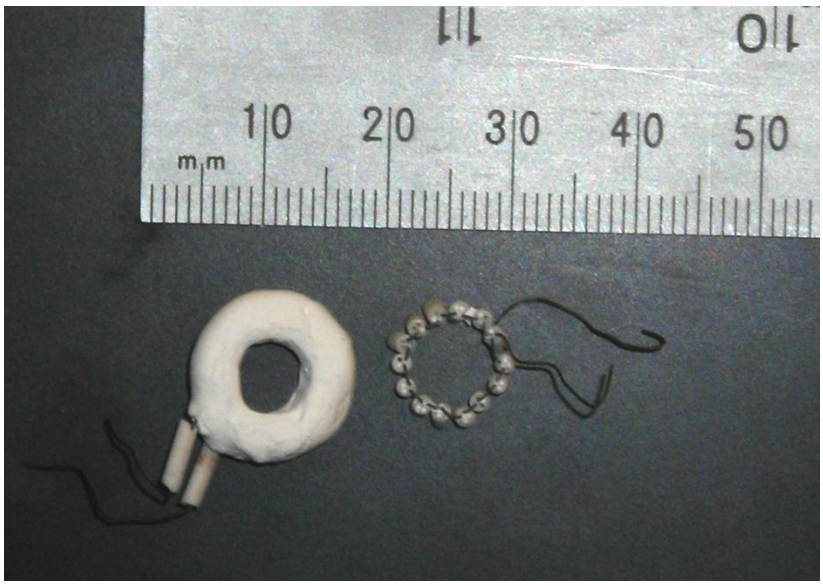

Figure 22. Second design - right heater is 4-hole tubing standing on end with wire threaded through each hole. Left heater is same design with alumina paste coating the outside.

The second design involved ceramic alumina tubing with four holes previously drilled through it. These tubes were cut to a specified height, roughly 2 mm, and placed the shape of a ring with the tubes standing

parallel to one another (Figure 22). Similar to the previous design, nichrome wire is threaded through all 4 holes of each of the tubes and attached to a power supply, creating a ring of wire-threaded tubing that is placed around the sample chamber of the diamond cell. An alumina paste was applied around the exposed wires at the end of the tubes in an effort to prevent them from touching each other and shorting out the whole system however it seemed like this did not prevent the wires from shorting out. The design initially worked, but when the wires got hot enough, they expanded and because they were already in such close proximity to each other, the small degree of thermal expansion was enough to cause them to touch and become ineffective. There was also a similar problem to the first design as there was no way to directly measure the temperature of the sample chamber.

Lastly, an external heater design was constructed. The 4-hole alumina tubing was placed in a square shape in two layers, and the nichrome wire was threaded through each layer and attached to the power supply (Figure 13). These heaters are placed outside the DAC and heat the cell as a whole. The heaters are spread further from each other in this design giving the added advantage of large temperature gradients throughout the whole system, ensuring that the measured temperature is more accurate.

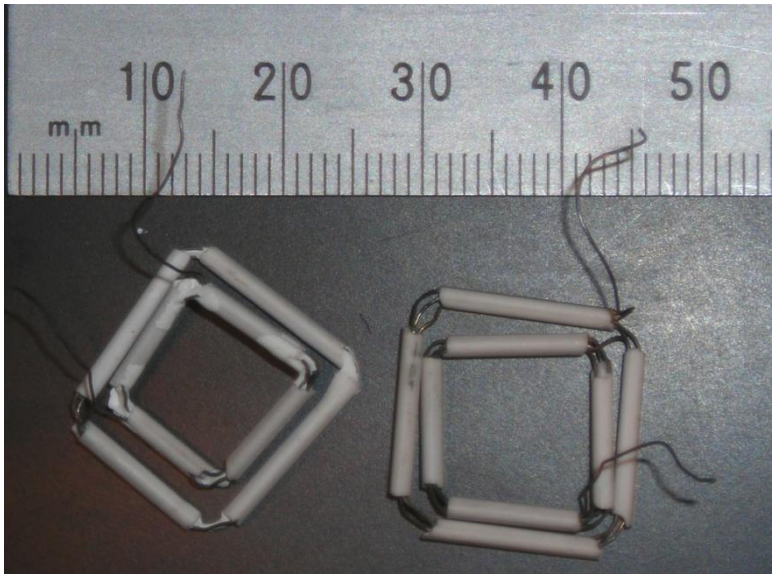

Figure 13. Final heater design. 4-hole tubing used in squares and placed outside the diamond anvil cell rather than inside.

Appendix B – Data

WO_2 Lattice Parameters with Pressure and Temperature

Pressure (GPa)	Temp (K)	WO2-a (Å)	WO2-a-error	WO2-b (Å)	WO2-b-error	WO2-c (Å)	WO2-c-error	WO2-β	WO2-β-error
2.27	675	5.578	0.009	4.910	0.008	5.642	0.007	120.95	0.08
2.30	675	5.574	0.004	4.895	0.005	5.653	0.006	120.78	0.07
2.41	675	5.604	0.006	4.855	0.007	5.704	0.005	121.10	0.12
2.77	675	5.610	0.010	4.847	0.013	5.711	0.022	121.01	0.24
4.28	485	5.576	0.003	4.880	0.005	5.657	0.005	121.08	0.05
7.59	300	5.545	0.015	4.847	0.010	5.640	0.015	121.09	0.25
9.97	575	5.545	0.002	4.816	0.004	5.659	0.004	120.95	0.05
10.07	575	5.553	0.008	4.841	0.012	5.658	0.015	121.21	0.21
11.61	472	5.536	0.011	4.829	0.005	5.638	0.012	121.57	0.17
12.72	375	5.504	0.033	4.801	0.009	5.624	0.011	121.53	0.19
13.12	300	5.504	0.033	4.783	0.011	5.622	0.027	121.40	0.40
13.15	300	5.492	0.006	4.792	0.003	5.597	0.002	121.21	0.08
18.58	625	5.491	0.011	4.769	0.004	5.577	0.009	122.04	0.15
19.83	575	5.444	0.005	4.763	0.004	5.567	0.006	121.70	0.08
23.31	475	5.386	0.011	4.759	0.006	5.553	0.011	122.47	0.17
24.99	300	5.379	0.024	4.745	0.005	5.533	0.010	122.00	0.11
25.00	300	5.402	0.015	4.723	0.010	5.526	0.009	121.51	0.16
25.35	300	5.397	0.009	4.714	0.008	5.507	0.007	121.53	0.12
25.62	375	5.344	0.012	4.744	0.003	5.539	0.007	121.99	0.12
26.68	575	5.379	0.004	4.737	0.006	5.487	0.004	121.32	0.07
31.75	715	5.340	0.016	4.714	0.013	5.513	0.010	121.76	0.25
32.11	715	5.403	0.010	4.689	0.004	5.548	0.004	122.73	0.08
35.13	375	5.368	0.009	4.671	0.013	5.516	0.010	123.05	0.18
37.45	300	5.339	0.014	4.688	0.014	5.516	0.009	123.48	0.21
41.50	300	5.279	0.002	4.659	0.001	5.504	0.002	122.57	0.04

WO_2 Volume With Pressure and Temperature

Pressure (GPa) (Gadf(GPa))	Temperature (K)	Volume (Å^3)	Volume error	Volume (cc/mol)	Volume error
2.27	675	132.51	0.26	19.95	0.04
2.30	675	132.52	0.13	19.95	0.02
2.41	675	132.86	0.15	20.00	0.02
2.77	675	133.11	0.26	20.04	0.04
4.28	485	131.85	0.10	19.85	0.02
7.59	300	129.81	0.39	19.54	0.06
9.97	575	129.60	0.08	19.51	0.01
10.07	575	130.09	0.30	19.58	0.04
11.61	472	128.42	0.26	19.33	0.04
12.72	375	126.82	0.31	19.09	0.05
13.12	300	126.34	0.78	19.02	0.12
13.15	300	126.00	0.10	18.97	0.02
18.58	625	123.80	0.22	18.64	0.03
19.83	575	122.80	0.14	18.49	0.02
23.31	475	120.09	0.28	18.08	0.04
24.99	300	119.77	0.48	18.03	0.07
25.00	300	120.22	0.34	18.10	0.05
25.35	300	119.41	0.18	17.98	0.03
25.62	375	119.10	0.26	17.93	0.04
26.68	575	119.42	0.13	17.98	0.02
31.75	715	117.99	0.38	17.76	0.06
32.11	715	118.26	0.17	17.80	0.03
35.13	375	115.92	0.24	17.45	0.04
37.45	300	115.15	0.29	17.34	0.04
41.50	300	114.08	0.04	17.17	0.01

NaCl B1 Crystal Structure Pressure Calibration

Temperature (K)	NaCl – a (Å)	NaCl - a - error	Pressure (GPa)
675	5.557	0.001	2.27
675	5.555	0.002	2.30
675	5.548	0.005	2.41
675	5.526	0.013	2.77
485	5.422	0.004	4.28
300	5.281	0.003	7.59
575	5.234	0.002	9.97
575	5.231	0.002	10.07
472	5.184	0.001	11.61
375	5.152	0.002	12.72
300	5.138	0.002	13.12
300	5.137	0.003	13.15
625	5.050	0.005	18.58
575	5.026	0.002	19.83
475	4.968	0.002	23.31
300	4.937	0.002	24.99
300	4.937	0.002	25.00
300	4.932	0.007	25.35
375	4.932	0.003	25.62

NaCl B2 Crystal Structure Pressure Calibration

Temperature (K)	NaCl-a (Å)	NaCl-a-error	Pressure (GPa)
300	2.9509	0.0048	41.50
715	3.0192	0.0005	32.11
715	3.0218	0.0028	31.75
575	3.0559	0.0063	26.68
375	2.9900	0.0025	35.13
300	2.9740	0.0051	37.45

WO_3 Lattice Parameters with Pressure

Pressure (GPa)	WO3-a (Å)	WO3-a-error	WO3-b (Å)	WO3-b-error	WO3-c (Å)	WO3-c-error	WO3-β	WO3-beta-error
10.7	5.124	0.003	4.752	0.002	7.280	0.002	95.50	0.04
16.3	5.104	0.003	4.663	0.002	7.181	0.003	96.47	0.05
20.1	5.081	0.005	4.603	0.003	7.109	0.005	97.11	0.09
22.9	5.065	0.004	4.565	0.003	7.064	0.004	97.43	0.07
25.0	6.168	0.006	4.588	0.004	5.317	0.005	101.45	0.09
29.0	6.146	0.008	4.556	0.005	5.304	0.006	101.28	0.10
29.6	6.107	0.004	4.562	0.002	5.311	0.003	101.88	0.06
32.8	6.112	0.004	4.545	0.002	5.289	0.002	101.65	0.04
34.8	10.391	0.008	3.944	0.002	9.353	0.009	99.96	0.09
40.8	10.325	0.006	3.906	0.002	9.280	0.005	99.76	0.07
44.5	10.291	0.008	3.877	0.002	9.211	0.006	99.26	0.05

WO_3 Volume with Pressure

Pressure (GPa)	Volume (Å^3)	Volume error	Volume (cc/mol)	Volume error
10.7	176.44	0.09	26.56	0.01
16.3	169.84	0.11	25.57	0.02
20.1	164.97	0.17	24.84	0.02
22.9	161.94	0.14	24.38	0.02
25.0	147.50	0.17	22.21	0.03
29.0	145.66	0.19	21.93	0.03
29.6	144.78	0.10	21.80	0.01
32.8	143.91	0.08	21.67	0.01
34.8	125.84	0.37	18.95	0.06
40.8	122.93	0.26	18.51	0.04
44.5	120.89	0.30	18.20	0.05

Argon Pressure Calibration

Ar-a	Ar-a-error	Pressure (GPa)
4.454	0.002	10.7
4.328	0.002	16.3
4.243	0.003	20.1
4.197	0.003	22.9
4.148	0.003	25.0
4.118	0.002	29.0
4.105	0.002	29.6
4.087	0.002	32.8
4.056	0.002	34.8
3.999	0.004	40.8
3.970	0.002	44.5

h-k-l Assignments for Diffraction Patterns

Pattern	P	Amp	2-Θ	d(Å)	h	k	l	d (calc)	Δd	Δd^2	sum of Δd^2	parameters	value	sigma
WO2-1	13.15	28	6.9	3.3867	0	1	1	3.3869	-0.0002	3.62E-08		a	5.492	*0.006*
		1	8.3	2.7975	-1	0	2	2.7985	-0.0010	9.84E-07	5.62E-06	b	4.792	*0.003*
		6	9.7	2.3957	0	2	0	2.3962	-0.0005	2.75E-07		c	5.597	*0.002*
		3	9.9	2.3485	2	0	0	2.3487	-0.0001	1.97E-08		β	121.212	*0.080*
		3	13.6	1.7139	-2	1	3	1.7124	0.0014	2.08E-06		V	126.004	*0.102*
		6	13.8	1.6949	0	2	2	1.6934	0.0015	2.23E-06				
WO2-2	2.41	9	6.8	3.4431	0	1	1	3.4431	0.0000	8.87E-10		a	5.604	*0.006*
		2	8.2	2.8521	-1	0	2	2.8520	0.0001	1.89E-08	2.85E-05	b	4.855	*0.007*
		5	9.6	2.4265	-2	1	1	2.4258	0.0007	4.83E-07		c	5.704	*0.005*
		6	13.6	1.7217	0	2	2	1.7216	0.0001	1.27E-08		β	121.104	*0.124*
		3	13.7	1.7027	2	2	0	1.7063	-0.0036	1.28E-05		V	132.863	*0.154*
		2	14.6	1.6003	3	0	0	1.5993	0.0010	9.71E-07				
		2	17.2	1.3582	-3	2	3	1.3594	-0.0012	1.32E-06				
		2	17.4	1.3450	2	3	0	1.3415	0.0035	1.23E-05				
		2	17.5	1.3348	3	2	0	1.3355	-0.0007	5.40E-07				
WO2-3	2.27	15	6.8	3.4452	0	1	1	3.4464	-0.0012	1.52E-06		a	5.578	*0.009*
		2	9.6	2.4415	-2	0	2	2.4404	0.0011	1.25E-06	3.37E-05	b	4.910	*0.008*
		3	9.6	2.4197	0	0	2	2.4193	0.0005	2.38E-07		c	5.642	*0.007*
		4	13.6	1.7228	0	2	2	1.7232	-0.0004	1.57E-07		β	120.947	*0.082*
		3	13.7	1.7032	1	1	2	1.7027	0.0004	1.76E-07		V	132.514	*0.262*
		3	15.2	1.5414	-3	1	3	1.5443	-0.0029	8.67E-06				
		3	15.8	1.4761	-2	2	3	1.4768	-0.0007	5.02E-07				
		4	19.0	1.2300	-2	3	3	1.2254	0.0046	2.11E-05				
		2	20.1	1.1622	4	1	0	1.1619	0.0002	5.70E-08				

WO2-4	2.77	11	6.8	3.4467	0	1	1	3.4441	0.0026	6.59E-06		a	5.610	*0.010*
		5	9.6	2.4273	-2	1	1	2.4272	0.0001	1.17E-08	4.65E-05	b	4.847	*0.013*
		4	13.6	1.7209	0	2	2	1.7221	-0.0012	1.34E-06		c	5.711	*0.022*
		2	15.1	1.5464	0	1	3	1.5464	0.0000	7.65E-12		β	121.006	*0.243*
		3	16.0	1.4612	1	2	2	1.4618	-0.0005	2.96E-07		V	133.107	*0.255*
		4	19.2	1.2220	-2	3	3	1.2225	-0.0006	3.30E-07				
		2	20.0	1.1684	3	2	1	1.1684	0.0000	3.68E-11				
		2	20.5	1.1432	0	3	3	1.1480	-0.0049	2.38E-05				
		1	21.2	1.1071	-5	0	2	1.1108	-0.0038	1.41E-05				
WO2-5	2.3	6	6.8	3.4472	0	1	1	3.4477	-0.0005	2.04E-07		a	5.574	*0.004*
		5	9.6	2.4405	-2	0	2	2.4399	0.0005	2.75E-07	3.29E-05	b	4.895	*0.005*
		1	12.7	1.8407	-2	2	1	1.8388	0.0019	3.67E-06		c	5.653	*0.006*
		6	13.5	1.7238	0	2	2	1.7238	0.0000	1.42E-10		β	120.776	*0.068*
		8	17.4	1.3452	2	3	0	1.3483	-0.0032	9.94E-06		V	132.519	*0.135*
		8	17.5	1.3390	3	2	0	1.3371	0.0019	3.60E-06				
		9	17.5	1.3345	2	1	2	1.3343	0.0002	4.10E-08				
		4	18.0	1.2978	-4	1	3	1.2987	-0.0009	8.54E-07				
		5	18.3	1.2819	-4	1	1	1.2849	-0.0030	8.77E-06				
		10	19.1	1.2250	0	4	0	1.2237	0.0013	1.76E-06				
		11	19.3	1.2135	-3	3	1	1.2141	-0.0005	2.75E-07				
		7	19.5	1.1992	4	0	0	1.1973	0.0019	3.53E-06				
WO2-6	9.97	10	6.8	3.4179	0	1	1	3.4184	-0.0005	2.12E-07		a	5.545	*0.002*
		1	9.7	2.4028	-2	1	1	2.4020	0.0008	6.48E-07	3.22E-06	b	4.816	*0.004*
		1	9.8	2.3774	2	0	0	2.3779	-0.0005	2.26E-07		c	5.659	*0.004*
		2	18.1	1.2926	-4	1	3	1.2932	-0.0006	3.70E-07		β	120.945	*0.046*
		6	20.0	1.1698	1	2	3	1.1684	0.0013	1.77E-06		V	129.596	*0.081*

WO2-7	10.07	18	6.8	3.4184	0	1	1	3.4223	-0.0039	1.52E-05		a	5.553	*0.008*
		2	9.7	2.4080	-2	1	1	2.4077	0.0004	1.39E-07	9.54E-05	b	4.841	*0.012*
		2	16.5	1.4186	-2	0	4	1.4144	0.0042	1.73E-05		c	5.658	*0.015*
		1	16.7	1.4014	-2	3	1	1.3949	0.0065	4.25E-05		β	121.210	*0.214*
		2	16.9	1.3868	-4	0	2	1.3877	-0.0009	8.00E-07		V	130.088	*0.298*
		2	17.0	1.3781	2	0	2	1.3756	0.0025	6.24E-06				
		3	18.1	1.2926	-4	1	3	1.2962	-0.0036	1.31E-05				
WO2-8	11.61	40	6.8	3.4040	0	1	1	3.4057	-0.0018	3.08E-06		a	5.536	*0.011*
		5	9.7	2.4014	0	0	2	2.4017	-0.0004	1.36E-07	1.23E-05	b	4.829	*0.005*
		2	9.9	2.3578	2	0	0	2.3581	-0.0003	1.13E-07		c	5.638	*0.012*
		4	13.7	1.7040	0	2	2	1.7029	0.0012	1.38E-06		β	121.574	*0.169*
		4	13.9	1.6831	1	1	2	1.6816	0.0016	2.43E-06		V	128.418	*0.259*
		3	17.5	1.3360	0	2	3	1.3344	0.0016	2.53E-06				
		3	19.3	1.2155	-2	3	3	1.2141	0.0015	2.10E-06				
		1	19.5	1.2001	0	0	4	1.2009	-0.0008	5.67E-07				
		9	20.2	1.1585	1	2	3	1.1584	0.0001	5.53E-09				
WO2-9	12.732	30	6.9	3.3950	0	1	1	3.3925	0.0026	6.72E-06		a	5.510	*0.011*
		5	9.7	2.3977	0	0	2	2.3970	0.0007	5.00E-07	4.41E-05	b	4.801	*0.009*
		3	9.9	2.3476	2	0	0	2.3482	-0.0006	3.95E-07		c	5.624	*0.011*
		2	13.7	1.7104	-1	1	3	1.7125	-0.0022	4.66E-06		β	121.528	*0.187*
		6	13.8	1.6910	0	2	2	1.6962	-0.0052	2.72E-05		V	126.822	*0.311*
		3	18.1	1.2891	-4	1	3	1.2878	0.0013	1.62E-06				
		4	21.8	1.0740	0	2	4	1.0723	0.0018	3.10E-06				
WO2-10	13.12	11	6.9	3.3901	0	1	1	3.3877	0.0024	5.79E-06		a	5.504	*0.033*
		1	9.7	2.4016	0	0	2	2.3995	0.0021	4.47E-06	5.18E-05	b	4.783	*0.011*
		1	13.8	1.6894	0	2	2	1.6939	-0.0044	1.95E-05		c	5.622	*0.027*

		1	17.2	1.3619	2	0	2	1.3612	0.0007	5.48E-07		β	121.398	*0.401*
		1	19.6	1.1953	0	0	4	1.1997	-0.0045	2.02E-05		V	126.344	*0.775*
		1	19.8	1.1818	2	2	2	1.1830	-0.0012	1.33E-06				
		2	20.4	1.1484	-4	2	1	1.1484	0.0000	1.63E-10				
WO2-11	4.28	4	6.8	3.4396	0	1	1	3.4383	0.0013	1.76E-06		a	5.576	*0.003*
		1	9.5	2.4440	-2	0	2	2.4449	-0.0009	7.27E-07	2.50E-05	b	4.880	*0.005*
		1	9.6	2.4220	-2	1	1	2.4203	0.0017	2.92E-06		c	5.657	*0.005*
		1	9.8	2.3876	2	0	0	2.3879	-0.0003	7.17E-08		β	121.082	*0.050*
		1	13.5	1.7327	-2	1	3	1.7328	0.0000	1.05E-09		V	131.848	*0.103*
		1	13.6	1.7191	0	2	2	1.7191	0.0000	2.14E-10				
		1	13.8	1.6932	2	1	1	1.6922	0.0010	1.05E-06				
		1	16.6	1.4059	-2	3	1	1.4050	0.0009	7.80E-07				
		1	16.7	1.3985	1	3	1	1.4018	-0.0032	1.03E-05				
		2	19.4	1.2089	-4	2	2	1.2101	-0.0013	1.59E-06				
		1	19.5	1.1995	2	2	2	1.2019	-0.0024	5.75E-06				
WO2-12	7.59	48	6.8	3.4265	0	1	1	3.4212	0.0052	2.73E-05		a	5.545	*0.015*
		10	9.7	2.4150	0	0	2	2.4151	-0.0001	9.71E-09	1.31E-04	b	4.847	*0.010*
		3	9.8	2.3743	2	0	0	2.3744	-0.0001	3.86E-09		c	5.640	*0.015*
		84	13.7	1.7005	0	2	2	1.7106	-0.0102	1.03E-04		β	121.091	*0.250*
		2	18.3	1.2755	-4	1	1	1.2753	0.0002	3.26E-08		V	129.814	*0.392*
		3	19.3	1.2114	0	4	0	1.2116	-0.0002	4.11E-08				
		2	19.5	1.2029	-4	2	2	1.2029	-0.0001	7.60E-09				
WO2-13	25	144	7.0	3.3358	0	1	1	3.3356	0.0002	4.07E-08		a	5.402	*0.015*
		10	9.8	2.3828	-1	1	2	2.3848	-0.0020	4.09E-06	7.43E-05	b	4.723	*0.010*
		6	9.9	2.3585	0	0	2	2.3557	0.0028	8.00E-06		c	5.526	*0.009*
		3	13.9	1.6824	-2	2	2	1.6775	0.0049	2.45E-05		β	121.508	*0.162*
		17	14.0	1.6631	0	2	2	1.6678	-0.0047	2.23E-05		V	120.221	*0.341*

		5	18.0	1.3019	2	3	0	1.2997	0.0021	4.60E-06				
		5	18.2	1.2843	3	2	0	1.2872	-0.0029	8.47E-06				
		3	18.3	1.2769	-3	1	4	1.2784	-0.0015	2.34E-06				
WO2-14	24.99	34	7.0	3.3349	0	1	1	3.3366	-0.0017	2.98E-06		a	5.379	*0.024*
		8	9.8	2.3719	0	2	0	2.3727	-0.0008	6.03E-07	3.61E-05	b	4.745	*0.005*
		6	13.8	1.6935	-2	1	3	1.6944	-0.0010	9.32E-07		c	5.533	*0.010*
		10	14.0	1.6726	0	2	2	1.6683	0.0043	1.82E-05		β	121.999	*0.113*
		3	14.3	1.6380	1	1	2	1.6370	0.0010	9.72E-07		V	119.772	*0.477*
		17	19.6	1.1948	-2	3	3	1.1922	0.0026	6.99E-06				
		7	20.8	1.1278	1	2	3	1.1301	-0.0023	5.45E-06				
WO2-15	25.62	197	7.0	3.3387	0	1	1	3.3381	0.0006	3.76E-07		a	5.344	*0.012*
		79	9.8	2.3724	0	2	0	2.3719	0.0005	2.53E-07	3.06E-05	b	4.744	*0.003*
		31	13.8	1.6937	-2	1	3	1.6943	-0.0006	3.69E-07		c	5.539	*0.007*
		50	14.0	1.6711	0	2	2	1.6690	0.0021	4.41E-06		β	121.990	*0.116*
		7	15.6	1.4956	0	3	1	1.4986	-0.0030	9.20E-06		V	119.102	*0.262*
		10	16.7	1.4016	1	2	2	1.4042	-0.0026	6.64E-06				
		3	17.3	1.3548	1	3	1	1.3562	-0.0014	2.04E-06				
		4	17.8	1.3125	0	3	2	1.3117	0.0008	6.19E-07				
		3	18.0	1.2994	2	3	0	1.2968	0.0026	6.70E-06				
WO2-16	23.31	82	7.0	3.3397	0	1	1	3.3388	0.0009	7.75E-07		a	5.386	*0.011*
		34	9.8	2.3772	0	2	0	2.3797	-0.0025	6.42E-06	1.21E-04	b	4.759	*0.006*
		2	12.9	1.8049	-1	2	2	1.8067	-0.0018	3.18E-06		c	5.553	*0.011*
		18	13.7	1.7003	-2	1	3	1.7018	-0.0015	2.30E-06		β	122.474	*0.174*
		28	13.9	1.6766	0	2	2	1.6694	0.0072	5.25E-05		V	120.091	*0.280*
		6	14.2	1.6440	2	2	0	1.6432	0.0008	5.64E-07				
		7	15.5	1.5074	-1	3	1	1.5061	0.0013	1.74E-06				
		14	16.7	1.3965	1	2	2	1.4028	-0.0063	3.94E-05				

		5	17.1	1.3695	-2	3	1	1.3662	0.0033	1.07E-05				
		6	17.2	1.3568	1	3	1	1.3586	-0.0018	3.30E-06				
		5	17.4	1.3442	-4	0	2	1.3439	0.0003	8.32E-08				
WO2-17	19.83	65	6.9	3.3550	0	1	1	3.3584	-0.0033	1.11E-05		a	5.444	*0.005*
		30	9.8	2.3835	0	2	0	2.3813	0.0022	4.63E-06	8.04E-05	b	4.763	*0.004*
		6	10.1	2.3178	2	0	0	2.3159	0.0019	3.76E-06		c	5.567	*0.006*
		11	13.7	1.7078	-2	1	3	1.7043	0.0035	1.20E-05		β	121.702	*0.080*
		22	13.9	1.6796	0	2	2	1.6792	0.0005	2.10E-07		V	122.805	*0.140*
		3	15.5	1.5098	-1	3	1	1.5075	0.0024	5.54E-06				
		1	17.2	1.3559	-4	0	2	1.3598	-0.0038	1.45E-05				
		1	18.1	1.2907	2	1	2	1.2905	0.0002	5.16E-08				
		5	19.6	1.1947	-2	3	3	1.1978	-0.0031	9.70E-06				
		3	19.7	1.1877	0	4	0	1.1907	-0.0030	8.86E-06				
		3	20.9	1.1226	0	3	3	1.1195	0.0032	1.00E-05				
WO2-18	18.58	135	6.9	3.3570	0	1	1	3.3574	-0.0004	1.55E-07		a	5.491	*0.011*
		47	9.8	2.3847	0	2	0	2.3845	0.0002	3.65E-08	5.58E-05	b	4.769	*0.004*
		8	10.0	2.3277	2	0	0	2.3275	0.0002	6.16E-08		c	5.577	*0.009*
		23	13.7	1.7100	-2	1	3	1.7099	0.0001	1.05E-08		β	122.037	*0.146*
		33	13.9	1.6840	0	2	2	1.6787	0.0053	2.81E-05		V	123.797	*0.219*
		5	15.5	1.5053	0	3	1	1.5068	-0.0015	2.21E-06				
		8	16.5	1.4142	1	2	2	1.4178	-0.0036	1.30E-05				
		2	17.0	1.3770	-2	3	1	1.3754	0.0017	2.74E-06				
		4	19.5	1.1975	-2	3	3	1.2006	-0.0031	9.50E-06				
WO2-19	25.35	196	7.0	3.3240	0	1	1	3.3259	-0.0020	3.88E-06		a	5.397	*0.009*
		113	9.8	2.3806	-1	1	2	2.3772	0.0033	1.12E-05	5.89E-05	b	4.714	*0.008*
		15	10.1	2.3009	2	0	0	2.3002	0.0007	4.98E-07		c	5.507	*0.007*
		13	13.0	1.7892	-1	2	2	1.7904	-0.0012	1.45E-06		β	121.532	*0.124*

		62	14.0	1.6672	0	2	2	1.6630	0.0043	1.82E-05		V	119.412	*0.178*
		19	16.7	1.4033	1	2	2	1.4062	-0.0029	8.34E-06				
		5	17.2	1.3584	-2	3	1	1.3576	0.0008	5.68E-07				
		7	18.4	1.2710	-3	1	4	1.2749	-0.0038	1.48E-05				
WO2-20	41.5	55	9.8	2.3688	-1	1	2	2.3692	-0.0004	1.73E-07		a	5.279	*0.002*
		13	10.0	2.3294	0	2	0	2.3295	-0.0001	1.70E-08	2.18E-06	b	4.659	*0.001*
		4	10.2	2.2919	-2	1	1	2.2923	-0.0004	1.70E-07		c	5.504	*0.002*
		1	13.4	1.7458	-2	2	1	1.7447	0.0010	1.09E-06		β	122.572	*0.041*
		33	14.0	1.6711	-1	1	3	1.6704	0.0007	5.11E-07		V	114.080	*0.044*
		10	14.2	1.6431	0	2	2	1.6435	-0.0005	2.20E-07				
WO2-21	32.11	11	9.8	2.3871	-1	1	2	2.3866	0.0005	2.54E-07		a	5.403	*0.010*
		2	13.0	1.7904	-1	2	2	1.7903	0.0001	1.09E-08	9.04E-06	b	4.689	*0.004*
		6	13.9	1.6796	-1	1	3	1.6804	-0.0008	6.16E-07		c	5.548	*0.004*
		2	17.4	1.3443	1	3	1	1.3428	0.0015	2.37E-06		β	122.732	*0.085*
		4	18.2	1.2856	2	3	0	1.2879	-0.0023	5.35E-06		V	118.256	*0.173*
		4	18.4	1.2732	3	2	0	1.2726	0.0007	4.41E-07				
WO2-22	31.75	36	9.8	2.3837	-1	1	2	2.3794	0.0043	1.85E-05		a	5.340	*0.016*
		2	13.0	1.7914	-1	2	2	1.7913	0.0001	5.45E-09	5.82E-05	b	4.714	*0.013*
		22	13.9	1.6748	-1	1	3	1.6791	-0.0042	1.78E-05		c	5.513	*0.010*
		2	17.4	1.3476	1	3	1	1.3502	-0.0026	6.78E-06		β	121.759	*0.249*
		3	18.3	1.2763	3	2	0	1.2735	0.0028	7.94E-06		V	117.992	*0.381*
		5	18.7	1.2501	-4	1	3	1.2528	-0.0027	7.19E-06				
WO2-23	26.68	56	9.8	2.3760	-1	1	2	2.3738	0.0021	4.56E-06		a	5.379	*0.004*
		13	10.0	2.3398	0	0	2	2.3436	-0.0037	1.38E-05	6.55E-05	b	4.737	*0.006*
		3	10.1	2.3003	2	0	0	2.2974	0.0028	7.99E-06		c	5.487	*0.004*
		2	13.0	1.7920	-1	2	2	1.7928	-0.0007	5.03E-07		β	121.319	*0.072*

		32	13.9	1.6778	-1	1	3	1.6742	0.0037	1.35E-05		V	119.425	*0.135*
		28	14.0	1.6709	-2	2	2	1.6744	-0.0035	1.20E-05				
		8	17.4	1.3416	-4	0	2	1.3438	-0.0023	5.08E-06				
		7	18.4	1.2698	-3	1	4	1.2701	-0.0003	1.09E-07				
		10	19.0	1.2345	-4	1	1	1.2358	-0.0012	1.52E-06				
		11	19.7	1.1889	-2	3	3	1.1863	0.0026	6.58E-06				
WO2-24	35.13	8	7.1	3.2838	0	1	1	3.2857	-0.0020	3.94E-06		a	5.368	*0.009*
		38	9.8	2.3731	-1	1	2	2.3735	-0.0004	1.97E-07	3.77E-05	b	4.671	*0.013*
		15	13.8	1.6924	-2	1	3	1.6906	0.0017	2.97E-06		c	5.516	*0.010*
		22	14.0	1.6702	-2	2	2	1.6706	-0.0004	1.46E-07		β	123.053	*0.185*
		3	17.5	1.3381	-4	0	2	1.3388	-0.0007	5.56E-07		V	115.923	*0.240*
		4	20.2	1.1571	1	3	2	1.1517	0.0055	2.99E-05				
WO2-25	37.45	6	7.1	3.2851	0	1	1	3.2835	0.0016	2.54E-06		a	5.339	*0.014*
		31	9.8	2.3702	-1	1	2	2.3756	-0.0054	2.91E-05	7.84E-05	b	4.688	*0.014*
		6	13.8	1.6973	-2	1	3	1.6921	0.0052	2.70E-05		c	5.516	*0.009*
		21	14.0	1.6656	-1	1	3	1.6677	-0.0021	4.42E-06		β	123.484	*0.212*
		2	14.5	1.6123	2	2	0	1.6143	-0.0020	4.06E-06		V	115.149	*0.288*
		3	19.7	1.1863	-2	3	3	1.1840	0.0023	5.28E-06				
		3	20.3	1.1526	0	0	4	1.1502	0.0025	6.02E-06				
Pattern	**P**	**Amp**	**2-Θ**	**d(Å)**	**h**	**k**	**l**	**d (calc)**	**Δd**	**Δd^2**	**sum of Δd^2**	**param**	**p-value**	**sigma**
WO3-1	10.7	65	6.4	3.6230	0	0	2	3.6233	-0.0003	7.61E-08		a	5.124	*0.003*
		116	6.7	3.4790	1	1	0	3.4768	0.0022	4.68E-06	4.91E-05	b	4.752	*0.002*
		15	8.1	2.8808	0	1	2	2.8813	-0.0006	3.55E-07		c	7.280	*0.002*
		9	8.2	2.8288	1	0	2	2.8285	0.0003	7.99E-08		β	95.501	*0.039*
		34	9.0	2.5934	-1	1	2	2.5948	-0.0014	1.85E-06		V	176.444	*0.091*

		18	9.6	2.4303	1	1	2	2.4306	-0.0003	8.85E-08				
		12	9.8	2.3743	0	2	0	2.3762	-0.0019	3.43E-06				
		5	10.8	2.1526	0	1	3	2.1533	-0.0008	5.86E-07				
		44	11.7	1.9889	0	2	2	1.9870	0.0019	3.44E-06				
		11	12.4	1.8851	-1	2	2	1.8853	-0.0002	3.92E-08				
		8	12.7	1.8400	2	1	2	1.8412	-0.0011	1.30E-06				
		4	12.9	1.8144	0	0	4	1.8116	0.0028	7.89E-06				
		15	13.8	1.6904	0	1	4	1.6928	-0.0024	5.84E-06				
		10	14.1	1.6531	-1	1	4	1.6514	0.0017	2.74E-06				
		25	14.5	1.6061	-2	2	2	1.6089	-0.0028	7.95E-06				
		13	15.4	1.5150	-3	1	2	1.5156	-0.0005	3.00E-07				
		14	15.9	1.4738	-2	1	4	1.4724	0.0014	1.97E-06				
		15	16.5	1.4128	-1	3	2	1.4104	0.0025	6.21E-06				
		12	18.6	1.2590	3	2	2	1.2594	-0.0005	2.35E-07				
		11	18.9	1.2412	2	3	2	1.2411	0.0001	1.98E-08				
WO3-2	16.3	66	6.5	3.5674	0	0	2	3.5678	-0.0004	1.98E-07		a	5.104	*0.003*
		105	6.8	3.4352	1	1	0	3.4327	0.0025	6.03E-06	1.16E-04	b	4.663	*0.002*
		18	8.2	2.8341	0	1	2	2.8336	0.0005	2.48E-07		c	7.181	*0.003*
		15	8.4	2.7760	1	0	2	2.7747	0.0013	1.70E-06		β	96.469	*0.050*
		35	9.1	2.5768	-1	1	2	2.5737	0.0031	9.68E-06		V	169.842	*0.112*
		24	9.2	2.5373	2	0	0	2.5358	0.0015	2.32E-06				
		18	9.8	2.3856	1	1	2	2.3845	0.0011	1.12E-06				
		10	10.0	2.3308	0	2	0	2.3317	-0.0009	7.99E-07				
		15	11.8	1.9781	-2	1	2	1.9797	-0.0016	2.65E-06				
		15	11.9	1.9621	2	0	2	1.9650	-0.0029	8.68E-06				
		28	12.3	1.8918	1	1	3	1.8888	0.0030	8.96E-06				
		12	12.5	1.8609	-1	2	2	1.8604	0.0005	2.65E-07				
		13	13.6	1.7145	2	2	0	1.7164	-0.0018	3.39E-06				
		11	14.0	1.6645	0	1	4	1.6662	-0.0016	2.65E-06				

		4	14.3	1.6335	-1	1	4	1.6348	-0.0012	1.45E-06				
		31	14.7	1.5903	-2	2	2	1.5949	-0.0047	2.18E-05				
		15	15.6	1.5005	2	2	2	1.5026	-0.0021	4.43E-06				
		17	15.7	1.4848	1	3	0	1.4862	-0.0014	2.02E-06				
		13	16.0	1.4641	-1	3	1	1.4647	-0.0005	2.76E-07				
		3	16.2	1.4434	1	3	1	1.4455	-0.0021	4.28E-06				
		10	16.8	1.3938	-1	3	2	1.3883	0.0055	3.03E-05				
		7	16.9	1.3864	2	0	4	1.3873	-0.0010	9.37E-07				
		8	17.3	1.3548	-1	1	5	1.3549	-0.0001	1.75E-08				
		10	17.5	1.3334	1	2	4	1.3340	-0.0006	3.95E-07				
		12	17.6	1.3289	2	1	4	1.3297	-0.0009	7.79E-07				
		8	18.2	1.2859	-2	2	4	1.2868	-0.0010	9.28E-07				
		11	18.9	1.2403	3	2	2	1.2406	-0.0002	5.00E-08				
WO3-3	20.1	70	6.6	3.5259	0	0	2	3.5271	-0.0012	1.48E-06		a	5.081	*0.005*
		98	6.9	3.3951	1	1	0	3.3993	-0.0041	1.72E-05	2.84E-04	b	4.603	*0.003*
		19	8.3	2.8010	0	1	2	2.7996	0.0014	2.06E-06		c	7.109	*0.005*
		8	8.5	2.7330	1	0	2	2.7355	-0.0025	6.24E-06		β	97.108	*0.087*
		51	9.1	2.5571	-1	1	2	2.5565	0.0006	3.50E-07		V	164.969	*0.166*
		27	9.2	2.5240	2	0	0	2.5210	0.0030	9.00E-06				
		25	9.9	2.3511	1	1	2	2.3515	-0.0005	2.19E-07				
		9	10.1	2.3023	0	2	0	2.3013	0.0011	1.10E-06				
		6	11.9	1.9689	1	2	1	1.9795	-0.0106	1.12E-04				
		14	12.1	1.9328	0	2	2	1.9273	0.0055	2.99E-05				
		2	12.7	1.8417	-1	2	2	1.8423	-0.0007	4.27E-07				
		8	13.8	1.6979	2	2	0	1.6996	-0.0017	3.06E-06				
		14	14.2	1.6476	0	1	4	1.6468	0.0008	6.54E-07				
		7	14.6	1.6037	1	0	4	1.6040	-0.0003	7.90E-08				
		23	14.8	1.5788	3	1	0	1.5787	0.0001	2.23E-08				
		11	15.7	1.4890	2	2	2	1.4835	0.0055	2.99E-05				

		11	15.9	1.4690	1	3	0	1.4677	0.0012	1.56E-06				
		14	16.1	1.4523	-1	3	1	1.4474	0.0049	2.44E-05				
		3	16.3	1.4322	-2	2	3	1.4355	-0.0033	1.06E-05				
		12	16.9	1.3828	3	1	2	1.3823	0.0005	2.57E-07				
		7	17.1	1.3689	2	0	4	1.3678	0.0011	1.21E-06				
		14	17.8	1.3117	-3	2	2	1.3114	0.0003	8.93E-08				
		11	18.8	1.2480	3	1	3	1.2454	0.0025	6.45E-06				
		11	19.0	1.2304	1	3	3	1.2254	0.0050	2.52E-05				
WO3-4	22.9	55	6.7	3.5020	0	0	2	3.5023	-0.0003	6.27E-08		a	5.065	*0.004*
		83	6.9	3.3762	1	1	0	3.3780	-0.0018	3.22E-06	8.15E-05	b	4.565	*0.003*
		13	8.4	2.7795	0	1	2	2.7787	0.0008	6.08E-07		c	7.064	*0.004*
		6	8.6	2.7157	1	0	2	2.7128	0.0029	8.47E-06		β	97.430	*0.073*
		35	9.2	2.5448	-1	1	2	2.5444	0.0004	1.24E-07		V	161.940	*0.136*
		16	9.3	2.5119	2	0	0	2.5110	0.0009	8.38E-07				
		13	10.0	2.3306	1	1	2	2.3321	-0.0015	2.35E-06				
		6	10.2	2.2850	0	2	0	2.2825	0.0026	6.70E-06				
		3	11.9	1.9632	1	2	1	1.9637	-0.0005	2.35E-07				
		6	13.8	1.6869	2	2	0	1.6890	-0.0021	4.37E-06				
		11	14.3	1.6357	0	1	4	1.6350	0.0007	4.96E-07				
		5	14.7	1.5898	1	0	4	1.5908	-0.0010	9.88E-07				
		14	14.9	1.5723	3	1	0	1.5717	0.0006	4.01E-07				
		7	17.0	1.3784	-1	2	4	1.3758	0.0026	6.75E-06				
		7	17.1	1.3664	-1	3	2	1.3629	0.0035	1.23E-05				
		5	17.6	1.3325	-1	1	5	1.3358	-0.0033	1.12E-05				
		3	17.7	1.3231	1	3	2	1.3271	-0.0040	1.60E-05				
		11	18.0	1.3026	1	2	4	1.3051	-0.0025	6.42E-06				
WO3-5	25.0	5	6.4	3.6681	1	1	0	3.6549	0.0131	1.73E-04		a	6.168	*0.006*
		72	6.8	3.4401	0	1	1	3.4438	-0.0037	1.40E-05	4.43E-04	b	4.588	*0.004*

		16	7.3	3.1805	-1	1	1	3.1771	0.0034	1.15E-05		c	5.317	*0.005*
		6	8.1	2.8690	-2	0	1	2.8742	-0.0052	2.68E-05		β	101.455	*0.092*
		6	8.2	2.8365	1	1	1	2.8365	0.0000	2.47E-09		V	147.501	*0.168*
		21	8.9	2.6090	0	0	2	2.6058	0.0032	1.04E-05				
		11	9.2	2.5247	2	1	0	2.5242	0.0005	2.43E-07				
		3	10.2	2.2898	0	2	0	2.2942	-0.0044	1.90E-05				
		5	10.3	2.2610	0	1	2	2.2659	-0.0049	2.41E-05				
		16	10.9	2.1368	2	1	1	2.1370	-0.0001	1.96E-08				
		7	11.7	1.9878	-2	1	2	1.9850	0.0028	7.74E-06				
		6	12.1	1.9305	1	2	1	1.9361	-0.0056	3.09E-05				
		5	12.7	1.8406	3	1	0	1.8451	-0.0045	2.01E-05				
		3	12.9	1.8083	2	0	2	1.8044	0.0039	1.56E-05				
		12	13.6	1.7173	-1	2	2	1.7165	0.0008	7.16E-07				
		7	14.1	1.6542	-3	1	2	1.6543	-0.0001	1.21E-08				
		9	14.3	1.6295	0	1	3	1.6246	0.0048	2.33E-05				
		6	14.6	1.5989	1	2	2	1.6016	-0.0027	7.45E-06				
		6	16.3	1.4359	4	1	0	1.4355	0.0004	1.89E-07				
		7	16.6	1.4057	1	3	1	1.4082	-0.0025	6.36E-06				
		10	16.9	1.3831	0	2	3	1.3849	-0.0018	3.21E-06				
		10	17.8	1.3127	-1	3	2	1.3166	-0.0039	1.48E-05				
		9	19.5	1.2017	4	0	2	1.2074	-0.0058	3.34E-05				
WO3-6	29.0	89	6.8	3.4278	0	1	1	3.4273	0.0005	2.77E-07		a	6.146	*0.008*
		19	7.4	3.1685	-1	1	1	3.1594	0.0091	8.21E-05	3.61E-04	b	4.556	*0.005*
		5	8.2	2.8547	-2	0	1	2.8617	-0.0070	4.93E-05		c	5.304	*0.006*
		6	8.2	2.8288	1	1	1	2.8269	0.0019	3.51E-06		β	101.277	*0.104*
		22	9.0	2.5987	0	0	2	2.6007	-0.0020	4.04E-06		V	145.661	*0.194*
		8	9.6	2.4248	-2	1	1	2.4234	0.0015	2.12E-06				
		16	10.9	2.1321	1	2	0	2.1310	0.0011	1.11E-06				
		6	11.8	1.9790	-2	1	2	1.9756	0.0034	1.14E-05				

		6	12.2	1.9199	1	2	1	1.9258	-0.0058	3.40E-05				
		2	12.9	1.8122	-2	2	0	1.8173	-0.0052	2.69E-05				
		11	13.7	1.7073	-1	2	2	1.7072	0.0001	2.59E-09				
		6	14.1	1.6565	2	2	1	1.6559	0.0005	2.85E-07				
		7	14.2	1.6443	-3	1	2	1.6465	-0.0021	4.52E-06				
		10	14.4	1.6200	0	1	3	1.6204	-0.0004	1.91E-07				
		10	16.3	1.4383	4	1	0	1.4307	0.0076	5.82E-05				
		6	16.7	1.3995	1	3	1	1.3996	-0.0001	9.52E-09				
		12	16.9	1.3857	3	1	2	1.3886	-0.0029	8.67E-06				
		14	18.0	1.3008	-1	3	2	1.3086	-0.0078	6.06E-05				
		8	19.4	1.2094	4	0	2	1.2056	0.0038	1.43E-05				
WO3-7	29.6	85	6.8	3.4266	0	1	1	3.4284	-0.0018	3.35E-06		a	6.107	*0.004*
		21	7.4	3.1667	-1	1	1	3.1651	0.0017	2.73E-06	1.32E-04	b	4.562	*0.002*
		5	8.2	2.8577	-2	0	1	2.8569	0.0007	5.60E-07		c	5.311	*0.003*
		18	9.0	2.5984	0	0	2	2.5986	-0.0002	2.94E-08		β	101.880	*0.060*
		17	10.9	2.1309	1	2	0	2.1309	0.0000	6.10E-10		V	144.778	*0.096*
		6	12.1	1.9244	1	2	1	1.9227	0.0017	2.87E-06				
		2	12.9	1.8071	-2	2	0	1.8130	-0.0059	3.49E-05				
		2	13.1	1.7860	-2	2	1	1.7825	0.0035	1.23E-05				
		14	13.7	1.7080	-1	2	2	1.7105	-0.0025	6.13E-06				
		8	14.2	1.6503	2	2	1	1.6490	0.0013	1.64E-06				
		11	14.4	1.6192	0	1	3	1.6195	-0.0003	9.91E-08				
		7	14.7	1.5930	1	2	2	1.5915	0.0016	2.47E-06				
		8	15.5	1.5072	-3	2	1	1.5050	0.0022	4.88E-06				
		6	15.9	1.4711	1	3	0	1.4736	-0.0026	6.67E-06				
		9	16.3	1.4375	-1	3	1	1.4370	0.0005	2.56E-07				
		4	16.6	1.4097	2	2	2	1.4067	0.0030	9.14E-06				
		12	16.9	1.3872	3	2	1	1.3854	0.0018	3.34E-06				
		10	18.0	1.3025	4	1	1	1.3062	-0.0036	1.30E-05				

		9	18.2	1.2853	2	3	1	1.2824	0.0029	8.34E-06				
		5	19.4	1.2063	-4	2	2	1.2106	-0.0043	1.89E-05				
WO3-8	32.8	70	6.8	3.4154	0	1	1	3.4166	-0.0013	1.56E-06		a	6.112	*0.004*
		17	7.4	3.1563	-1	1	1	3.1536	0.0027	7.34E-06	6.55E-05	b	4.545	*0.002*
		14	9.0	2.5914	0	0	2	2.5902	0.0011	1.30E-06		c	5.289	*0.002*
		7	9.3	2.5004	2	1	0	2.4997	0.0007	4.79E-07		β	101.653	*0.043*
		7	9.7	2.4142	-2	1	1	2.4165	-0.0023	5.23E-06		V	143.910	*0.078*
		15	11.0	2.1242	1	2	0	2.1246	-0.0005	2.05E-07				
		7	11.8	1.9718	-2	1	2	1.9726	-0.0009	7.34E-07				
		8	12.2	1.9151	1	2	1	1.9181	-0.0030	8.93E-06				
		4	13.1	1.7812	-2	2	1	1.7776	0.0036	1.26E-05				
		12	13.7	1.7019	-1	2	2	1.7037	-0.0018	3.31E-06				
		10	14.2	1.6422	-3	1	2	1.6429	-0.0007	5.31E-07				
		11	14.5	1.6149	0	1	3	1.6142	0.0006	3.89E-07				
		8	14.7	1.5891	1	2	2	1.5878	0.0012	1.49E-06				
		10	16.3	1.4331	-1	3	1	1.4318	0.0012	1.55E-06				
		7	16.6	1.4054	2	2	2	1.4052	0.0001	1.91E-08				
		14	16.9	1.3849	3	2	1	1.3852	-0.0003	1.10E-07				
		12	17.5	1.3340	-2	2	3	1.3334	0.0006	4.00E-07				
		11	18.0	1.2989	1	2	3	1.2954	0.0035	1.24E-05				
		11	18.2	1.2858	-2	0	4	1.2871	-0.0014	1.85E-06				
		11	20.4	1.1459	3	3	1	1.1447	0.0013	1.57E-06				
		8	21.5	1.0905	1	3	3	1.0924	-0.0019	3.46E-06				
WO3-9	34.8	6	6.4	3.6235	0	1	1	3.6256	-0.0021	4.43E-06		a	10.391	*0.008*
		75	6.9	3.3963	-3	0	1	3.3961	0.0001	2.04E-08	2.59E-04	b	3.944	*0.002*
		8	8.3	2.8135	1	0	3	2.8105	0.0030	9.18E-06		c	9.353	*0.009*
		14	9.0	2.5770	-3	1	1	2.5735	0.0035	1.21E-05		β	99.960	*0.092*
		4	9.7	2.4003	3	1	1	2.4042	-0.0039	1.48E-05		V	377.530	*0.372*

		11	11.0	2.1130	-3	1	3	2.1165	-0.0035	1.20E-05				
		6	11.9	1.9539	-2	1	4	1.9550	-0.0011	1.19E-06				
		5	12.2	1.9098	-1	2	1	1.9075	0.0023	5.22E-06				
		3	12.5	1.8609	3	1	3	1.8592	0.0016	2.72E-06				
		3	12.6	1.8465	4	1	2	1.8457	0.0007	5.62E-07				
		2	12.7	1.8339	2	2	0	1.8401	-0.0061	3.78E-05				
		4	12.8	1.8193	0	2	2	1.8128	0.0065	4.23E-05				
		9	13.8	1.6923	-1	1	5	1.6902	0.0022	4.83E-06				
		5	14.0	1.6629	-1	2	3	1.6626	0.0003	7.97E-08				
		8	14.3	1.6288	-2	2	3	1.6235	0.0053	2.80E-05				
		8	14.5	1.6111	1	2	3	1.6142	-0.0032	1.00E-05				
		6	16.1	1.4547	1	2	4	1.4588	-0.0041	1.70E-05				
		10	16.4	1.4260	0	1	6	1.4308	-0.0048	2.35E-05				
		11	18.1	1.2950	-1	3	1	1.2950	-0.0001	5.47E-09				
		8	18.3	1.2760	2	3	0	1.2733	0.0028	7.58E-06				
		4	19.5	1.1986	-2	3	3	1.1945	0.0040	1.63E-05				
		9	20.6	1.1387	0	3	4	1.1417	-0.0030	9.17E-06				
		3	21.9	1.0698	0	3	5	1.0702	-0.0003	1.05E-07				
WO3-10	40.8	4	6.5	3.5873	0	1	1	3.5918	-0.0045	2.00E-05		a	10.325	*0.006*
		68	6.9	3.3689	-3	0	1	3.3719	-0.0030	9.15E-06	1.40E-04	b	3.906	*0.002*
		12	7.5	3.1019	2	1	0	3.0980	0.0039	1.50E-05		c	9.280	*0.005*
		7	8.4	2.7923	1	0	3	2.7932	-0.0009	8.02E-07		β	99.758	*0.067*
		13	9.1	2.5585	3	1	0	2.5609	-0.0023	5.42E-06		V	368.803	*0.255*
		4	9.8	2.3843	3	1	1	2.3879	-0.0037	1.34E-05				
		8	11.1	2.0959	-3	1	3	2.0975	-0.0017	2.72E-06				
		3	12.1	1.9369	-2	1	4	1.9377	-0.0009	7.48E-07				
		4	12.2	1.9151	1	2	0	1.9178	-0.0027	7.26E-06				
		3	12.4	1.8892	-1	2	1	1.8891	0.0001	4.44E-09				
		3	12.6	1.8510	3	1	3	1.8479	0.0031	9.92E-06				

		4	12.8	1.8287	0	0	5	1.8292	-0.0005	2.87E-07				
		3	13.9	1.6793	-1	1	5	1.6763	0.0030	8.93E-06				
		5	14.5	1.6146	-2	2	3	1.6083	0.0063	4.01E-05				
		8	14.6	1.5972	1	1	5	1.5966	0.0006	3.15E-07				
		5	15.7	1.4915	-1	2	4	1.4930	-0.0015	2.35E-06				
		10	18.2	1.2830	-1	3	1	1.2825	0.0005	2.88E-07				
		8	19.6	1.1959	0	3	3	1.1973	-0.0013	1.74E-06				
		4	20.7	1.1325	0	3	4	1.1313	0.0012	1.46E-06				
		3	21.0	1.1147	1	3	4	1.1142	0.0006	3.20E-07				
WO3-11	44.5	9	6.3	3.6964	-2	0	2	3.6954	0.0010	1.06E-06		a	10.291	*0.008*
		6	6.5	3.5643	0	1	1	3.5661	-0.0018	3.16E-06	1.70E-04	b	3.877	*0.002*
		69	7.0	3.3533	-3	0	1	3.3541	-0.0008	6.90E-07		c	9.211	*0.006*
		12	7.6	3.0774	2	1	0	3.0815	-0.0041	1.66E-05		β	99.263	*0.053*
		7	8.4	2.7805	1	0	3	2.7836	-0.0032	9.93E-06		V	362.682	*0.301*
		14	9.1	2.5494	3	1	0	2.5500	-0.0006	4.00E-07				
		8	11.2	2.0831	-3	1	3	2.0793	0.0039	1.50E-05				
		4	12.2	1.9168	-2	1	4	1.9209	-0.0040	1.64E-05				
		6	12.7	1.8349	4	1	2	1.8320	0.0029	8.39E-06				
		3	12.9	1.8063	-2	0	5	1.8066	-0.0003	7.69E-08				
		5	14.0	1.6648	-1	1	5	1.6637	0.0012	1.37E-06				
		5	14.1	1.6535	2	2	2	1.6501	0.0034	1.17E-05				
		1	14.3	1.6384	-2	1	5	1.6375	0.0009	8.46E-07				
		4	14.5	1.6061	3	1	4	1.6029	0.0032	1.05E-05				
		8	14.7	1.5934	1	2	3	1.5907	0.0027	7.41E-06				
		4	14.9	1.5729	4	0	4	1.5723	0.0006	3.86E-07				
		9	18.3	1.2799	-1	3	1	1.2730	0.0069	4.76E-05				
		4	19.3	1.2156	-2	3	2	1.2198	-0.0043	1.83E-05				

References

Bouvier, P. et al.; "X-ray diffraction study of WO_3 at high pressure." Journal of Physics: Condensed Matter 14 (2002) 6605-6617

Campbell, Andrew J., et. al.; "High pressure effects on the iron–iron oxide and nickel–nickel oxide oxygen fugacity buffers." Earth and Planetary Science Letters 286 (2009): 556-564

Cottrell, Elizabeth, et. al; . "Metal-silicate partitioning of tungsten at high pressure and temperature; implications for equilibrium core formation in Earth." Earth and Planetary Science Letters 281.3-4 (2009): 275-287.

Dorogokupets, Peter I., Oganov, Artem R.; "Ruby, metals, and MgO as alternative pressure scales: A semiemperical description of shock-wave, ultrasonic, x-ray, and thermochemical data at high temperatures and pressures." The American Physical Society. 024115-(1-6) (2007)

Fei et al. "Toward an internally consistent pressure scale." (2007) Proc. Nat. Acad. Sci., doi:10.1073/pnas.0609013104.]

Hillgren, Valerie J., et al.; . "High pressure and high temperature metal-silicate partitioning of siderophile elements; the importance of silicate liquid composition." Geochimica et Cosmochimica Acta 60.12 (1996): 2257-2263.

Howard, Christopher J., et al.; "High-temperature phase transitions in tungsten trioxide—the last word?" Journal of Physics: Condensed Matter 14 (2002): 377-387

Jacobsen, Steven D. "Diamon*d*-Anvil Cell (DAC)" Northwestern University, Department of Earth and Planetary Sciences. 2009 <http://www.earth.northwestern.edu/research/jacobsen/>

Komabayashi, Tetsuya et al.,: "In-situ X-ray diffraction measurements of the γ-ε transition boundary of iron in an internally-heated diamond anvil cell." Earth and Plantetary Science Letters 282 (2009): 252-257

Mao, H. K. et al., "Calibration of the ruby pressure gauge to 800 kbar under quasi-hydrostatic conditions." Journal of Geophysical Research v.91, no. B5, (1986) 4673-4676

O'Neill, Hugh St.C., et al.,: "The solubility and oxidation state of tungsten in silicate melts: Implications for the comparative chemistry of W and Mo in planetary differentiation processes." Chemical Geology 2008

Righter, Kevin, et al.; . "Metal-silicate partitioning of siderophile elements and core formation in the early Earth." Annual Review of Earth and Planetary Sciences 31 (2003): 135-174.

Rose-Weston, Lesley, et al.; . "Effect of pressure, temperature, and oxygen fugacity on the metal-silicate partitioning of Te, Se, and S; implications for Earth differentiation." Geochimica et Cosmochimica Acta 73.15 (2009): 4598-4615.

Shofner, Gregory, et al.: in preparation.

I pledge on my honor that I have not given or received any unauthorized assistance or plagiarized on this assignment.

TJ Deane